Journal of Cerebral Blood Flow & Metabolism (2012) 32, S13–S40
© 2012 ISCBFM All rights reserved 0271-678X/12 $32.00
www.jcbfm.com

Oral Presentation Abstracts

Journal of Cerebral Blood Flow & Metabolism (2012) **32,** S13–S40; doi:10.1038/jcbfm.2012.77

O1. Changes in striatal dopamine in response to IV alcohol in nontreatment-seeking alcoholics but not social drinkers

Karmen Yoder, Daniel Albrecht, Christine Herring, Lauren Federici, Elizabeth Patton, Sean O'Connor and David Kareken

Indiana University School of Medicine, Indianapolis, Indiana, USA

Background: The effects of oral and IV alcohol administration on striatal dopamine (DA) release have been studied in social drinkers, with equivocal results. However, the striatal DA system response to alcohol has not been studied in an alcoholic population. If alcoholics exhibit differential reactions of the DA system to alcohol, this could provide critical clues as to the neurobiological underpinnings of alcohol use disorders. Thus, the goals of this work were twofold: First, we sought to compare striatal DA responses to IV alcohol administration between nontreatment-seeking alcoholics (NTS) and social drinkers (SD). Second, we sought to determine the reproducibility of these effects.

Methods: Twenty right-handed male smokers (10 NTS, 10 SD) were studied with PET and [^{11}C]raclopride (RAC) to determine the effects of IV alcohol on relative striatal DA levels. Subjects received two pairs of RAC scans (rest, IV alcohol) on two separate days. During the alcohol RAC scan, pharmacokinetic modeling was used to deliver an intravenous infusion of alcohol to a target blood alcohol concentration of 80 mg%.

Results: No effects of IV alcohol on DA were found in SD on either Day 1 or Day 2, replicating our earlier findings in two other SD cohorts. In NTS subjects, IV alcohol resulted in reproducible increases in DA in the left anterior putamen, and reproducible decreases in DA in the right dorsal caudate. None of these effects were associated with either subjective responses to alcohol or alcohol craving.

Conclusions: The distinctive anatomic pattern of DA responses to IV alcohol in currently-drinking alcoholics may be indicative of dopamine-related cognitive processes involved in hazardous drinking behavior, such as coding for stimulus salience and/or habitual responding to the presence of alcohol.

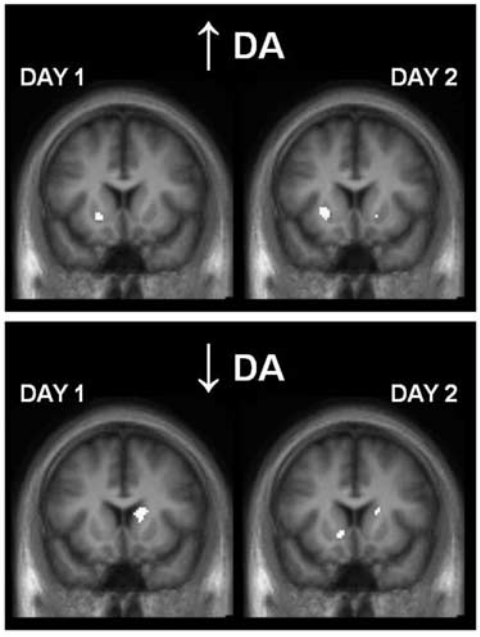

Figure Reproducible effects of IV alcohol to intoxication (80 mg%) on striatal dopamine (DA) in nontreatment-seeking alcoholics ($n = 10$) on study Day 1 (left) and Day 2 (right). Voxel-wise testing was paired t-tests between BP_{ND} from baseline and alcohol [^{11}C]raclopride scans on each respective study day. Voxels that met or exceeded display threshold of $p < 0.05$ (uncorrected) are shown in white. Top: Increases in DA in left anterior putamen. Bottom: Decreases in DA in the right dorsal caudate.

O2. Relationships of D1- and D2-like receptor availability and response inhibition in the stop-signal task: a preliminary PET study

Chelsea Robertson[1], Kenji Ishibashi[2], Amira Brown[2], Andrew Morgan[2,3], Dara Ghahremani[2], Eliza Congdon[2], Judah Farahi[3], Mark Mandelkern[3,4], Tyrone Cannon[5], Fred Sabb[2] and Edythe London[2,6]

[1]Department of Molecular and Medical Pharmacology at University of California at Los Angeles, USA; [2]Department of Psychiatry and Biobehavioral Sciences and Semel Institute at University of California at Los Angeles; [3]Veterans Administration Greater Los Angeles Healthcare System, California, USA; [4]Department of Physics at University of California at Irvine, USA; [5]Department of Psychology and Department of Psychiatry and Biobehavioral Sciences and Semel Institute at University of California at Los Angeles, USA; [6]Department of Molecular and Medical Pharmacology and Brain Research Institute at University of California at Los Angeles, USA

Background: Dopaminergic neurotransmission in the dorsal striatum is an essential component of the neural circuitry that mediates response inhibition. A recent animal study reports opposing roles for striatal D1- and D2-like receptors in response inhibition (1). These findings suggest a model in which D1- and D2-like receptors promote competing processes via modulation of the direct (go) and indirect (no-go) pathways, respectively (2). Therefore, individual variation in striatal D1- or D2-like receptor availability may relate to individual response inhibition capacity. Despite known associations of D2-like receptors and response inhibition (3), the relationship between D1-like receptors and response inhibition has not been tested. We hypothesized that individual differences in availability of both striatal D1- and D2-like receptors would be related to measurements of response-inhibition capacity. To test this hypothesis, we examined the relationship between performance on the Stop-signal task, a well-established test of response inhibition, and measurements of D1- and D2-like receptor availability using the PET radioligands ^{11}C-NNC-112 and ^{18}F-fallypride, respectively.

Methods: 15 healthy volunteers (8 men, mean age = 28.47, SD = 7.8) completed the stop-signal task and MRI scans. Nine participants underwent ^{11}C-NNC-112 PET scans for determination of caudate D1-like receptor binding potential (BP_{ND}) and twelve participants underwent ^{18}F-fallypride PET scans for determination of caudate D2-like BP_{ND}. BP_{ND} for each tracer was calculated using the Simplified Reference Tissue Model 2 (4) using the cerebellum as the reference region. Voxel-wise BP_{ND} maps for each radiotracer were generated in standard space (MNI). Capacity for response inhibition was indexed by stop-signal reaction time (SSRT). Partial correlations were performed (controlling for age) to assess the relationship between BP_{ND} and SSRT.

Results: VOI analyses showed a significant correlation between caudate D2 BP_{ND} for ^{18}F-fallypride and SSRT (r = -0.69, p = 0.019). However, D1 BP_{ND} for ^{11}C-NNC-112 was not significantly correlated with SSRT. Exploratory voxel-wise regression analysis of ^{18}F-fallypride BP_{ND} showed a negative relationship with SSRT in the dorsal striatum, at a liberal threshold due to small sample size ($p < 0.05$, uncorrected, Figure1). A similar voxel-wise regression analysis of ^{11}C-NNC-

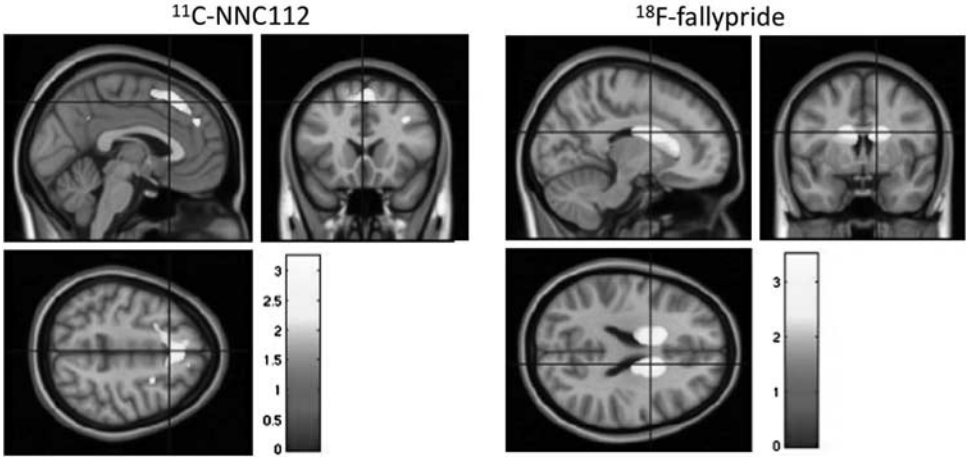

Figure 1 Voxel-wise regression analyses of ^{18}F-fallypride BP_{ND} showing a negative relationship with SSRT in the dorsal striatum (right) and ^{111}C-NNC-112 BP_{ND} showing a positive relationship with SSRT in the cortex (left) ($p < 0.05$, uncorrected). The scale bars represent *T* value.

112 BP_{ND} showed a positive relationship with SSRT in a cortical area extending from the pre-supplementary motor area to the superior frontal gyrus, at the same liberal threshold ($p < 0.05$, uncorrected, Figure 1).

Conclusions: Our results suggest that striatal D2-like receptors may contribute more than striatal D1-like receptors to the neurocircuitry of response inhibition. These results also provide preliminary evidence that D1-like receptors in the cortex play an important role in the neurocircuitry that underlies response inhibition.

Acknowledgements: Supported by the Consortium for Neuropsychiatric Phenomics (NIH Roadmap for Medical Research grants UL1-DE019580, RL1DA024853).

References

1. Eagle, *J Neurosci* 31:7344, 7349-7356 (2011).
2. Logan and Cowan, *J Exp Psychol Hum Percept Perform* 10:276-291 (1984).
3. Ghahremani, *J Neurosci* (in review).
4. Wu Y, *J Cereb Blood Flow Metabolism* 22:1440-1452 (2002).

O3. Diurnal changes in the available dopamine D2/D3 receptor density suggests decreased intrasynaptic dopamine at night

Hiroto Kuwabara[1], Christopher Earley[2], Weiguo Ye[1], Richard Allen[2], Maria Guevara[1] and Dean F. Wong[1]

Johns Hopkins University, Baltimore, Maryland, USA, Departments of: [1]Radiology; [2]Neurology

Background: Reported prolonged suppression of [^{11}C]raclopride binding potential (BP_{ND}) after amphetamine challenge suggested that physiological phasic discharges of dopamine (DA) during day-time could render DA D2/D3 receptors less accessible to [^{11}C]raclopride and cause decreased BP_{ND} at night compared to morning hours. This hypothesis was tested in this study.

Methods: Healthy middle-age subjects (41-65 years) were studied either in morning hours (8:30 AM; 56.1 ± 5.9 years; 5F/8M) or at night (9 PM; 53.8 ± 7.3 years; 8F/2M). Each subject had high- and low-specific activity [^{11}C]raclopride scans (HSA and LSA) and one [^{11}C]methylphenidate (MP, a marker for DA transporter) scan. PET outcome variables, BP_{ND}, the density of available D2/D3 receptors (B_{avail}), and the dissociation constant (K_D) were obtained by the bolus-plus-infusion transformation (BPIT) of bolus injection studies (JNM 2012) in limbic (ventral striatum; vS), associative (anterior putamen, aPu, and anterior and posterior caudate nucleus, aCN and pCN), and motor (posterior putamen, pPu) striatum which were defined on MRI.

Results: Injected mass of raclopride were not different between morning (M) and night (N) groups for HSA ($t = 1.2$; $p > 0.23$) and LSA (M: 14.1 ± 5.8 μmol/mCi; N: 16.3 ± 3.2 μmol/mCi; $t = 1.2$; $p > 0.25$) scans. B_{avail} was greater for N than M group in pPu (22%) and vS (37%) (ANOVA: group effect: $F = 4.75$; $p < 0.05$; t-test:

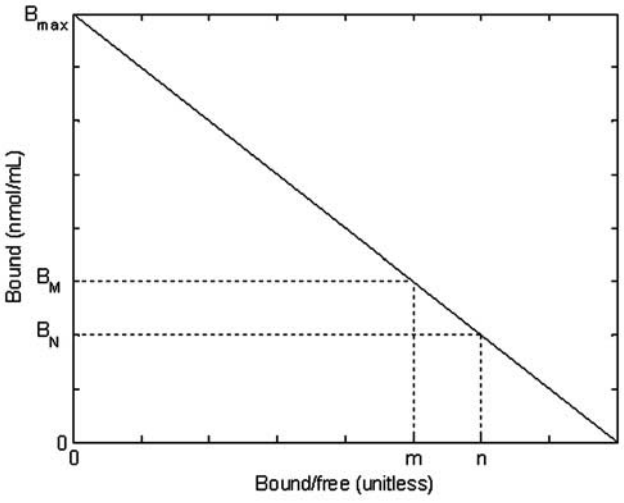

Figure Eadie-Hofstee plot showing DA receptors that were occupied by DA in morning (B_M) and at night (B_N). B_{avail} is given by B_{max} - B_M or B_{max} - B_N for morning or at night.

Table

		APu	pPu	aCN	pCN	vS
Baseline BP_{ND} (ratio)	Morning	2.69 ± 0.06	2.68 ± 0.06	2.40 ± 0.05	1.68 ± 0.07	1.68 ± 0.07
	Night	2.84 ± 0.08	3.04 ± 0.07	2.50 ± 0.07	1.80 ± 0.10	1.81 ± 0.10
B_{avail} (nmol/mL)	Morning	24.6 ± 1.5	25.9 ± 1.3	19.8 ± 1.3	14.6 ± 1.4	16.2 ± 1.3
	Night	29.4 ± 2.1	31.0 ± 2.3	24.2 ± 1.9	18.5 ± 2.0	22.2 ± 1.9
K_D (nmol/mL)	Morning	9.2 ± 0.5	9.2 ± 0.5	8.4 ± 0.5	8.7 ± 0.6	9.7 ± 0.8
	Night	10.4 ± 0.6	10.4 ± 0.8	9.7 ± 0.6	10.3 ± 0.9	12.4 ± 1.2

$p = 0.012$ vS; $p < 0.05$ for pPu). Baseline BP_{ND} of [^{11}C]raclopride (group effect: $F = 2.20$; $p = 0.147$) and [^{11}C]MP ($F = 0.25$; $p = 0.62$), and K_D ($F = 1.95$; $p = 0.173$) remained unchanged between groups. To understand the findings, the Eadie-Hofstee plot (x: bound/free; y: bound; y-intercept: B_{max} (the receptor density); and slope: $-K_D$) was extended to include bound DA receptors for groups N ($= B_N$) and M ($= B_M$) as shown.

Conclusions: Contrary to the hypothesis, B_{avail} were higher at night than morning without changes in K_D. The Eadie-Hofstee plot indicates that, to achieve observed increases in B_{avail} ($= B_{max} - B_M$ or $B_{max} - B_N$ for M and N groups), occupancy of DA receptors in morning must be greater than 18% for pPu and 27% for vS. Therefore, this model suggested that baseline occupancy of D2/D3 receptors by DA could be higher than commonly assumed (i.e., 10%).

O4. The relation between body mass index and dopamine D2 receptor availability in the caudate: a PET study in humans

Danielle Z. Bolling[1], Maria G. Veldhuizen[2], Kelly P. Cosgrove[3], Dana M. Small[2] and Evan D. Morris[4]

[1]Interdepartmental Neuroscience Program, Yale University, New Haven, Connecticut, USA; [2]John B. Pierce Laboratory, Yale School of Medicine; [3]Psychiatry Department, Yale University; [4]Radiology Department, Yale University

Background: Research on the neurobiology of obesity has suggested that dopamine (DA) plays an important role in the disorder by means of its relation to the rewarding and motivational effects of food consumption. Striatal dopamine levels are significantly related to eating behavior in humans (Palmiter, 2007; Wise, 2006). However, evidence exists suggesting that different sub-regions of the striatum may have differential roles in reward and motivational processes associated with food consumption (Small, 2003; Szczypka, 2001). A recent fMRI study demonstrated that activation in the caudate due to food consumption correlated inversely with body mass index (BMI) - higher BMI was associated with lower caudal activation (Stice, 2008). In addition, a PET imaging study demonstrated that in individuals with BMIs greater than 40, higher BMI correlated with lower DA D2 receptor (D2R) availability in the striatum (Wang, 2002). This and other findings are consistent with the hypothesis that obesity might be related to hypoactive neural reward circuitry. The current study aims to investigate the relationship between DA receptor availability and BMI in specific sub-regions of the striatum. We hypothesize that BMI will significantly correlate with D2R availability in the caudate, consistent with evidence emphasizing the role of dorsal striatum in obesity.

Methods: Eight adults (6 male, 27.4 ± 6.1 years) with BMIs ranging from 20.5 to 38.8 underwent PET scans on the HRRT using the D2R agonist tracer ^{11}C-PHNO. All data were acquired to a listmode file. Iterative reconstruction (MOLAR) was applied with all corrections including event-by-event motion correction (Polaris system).The scan began with a bolus injection (or infusion) of the radioligand, and lasted for 120 minutes. For specific striatal regions of interest, time activity curves were extracted, and binding potentials (BP_{ND}) were calculated using the simplified reference tissue model (SRTM) with the cerebellum as a reference region.

Results: Binding potentials in right dorsal caudate showed a significant positive correlation with BMI such that individuals with higher BMIs had increased radioligand binding in this region ($R^2 = 0.62$). A similar correlation was trending towards significance in bilateral dorsal caudate ($R^2 = 0.46$). Binding potentials in these two regions did not correlate significantly with age. BMI also showed no significant relationship with age.

Conclusions: In contrast with past PET imaging findings, we found that individuals with higher BMIs showed higher D2R availability in striatum, specifically the right caudate. Discrepancies between the present and previous results may arise from a number of experimental factors. We used the agonist tracer PHNO, while the previous study used raclopride. We assayed individual striatal sub-regions, while the earlier study reported results from whole striatum. The previous report investigated a higher, non-overlapping range of BMI (previous subjects were morbidly obese). Thus, the innovations of present study have the potential to shed light on the complexities of the relation between BMI and D2R receptor availability in sub-regions of the striatum.

O5. Evaluation of a small library of carbamates and ureas, including PF-04457845, as potential imaging agents for fatty acid amide hydrolase (FAAH)

Justin Hicks[1], Oleg Sadovski[1], Jun Parkes[1], Chris Fowler[2], Sylvain Houle[1], Junchao Tong[1], Neil Vasdev[3] and Alan Wilson[1]

[1]Centre for Addiction and Mental Health,Toronto, Canada; [2]Umea University, Sweden; [3]Mass General Hospital, Boston, Massachusetts, USA

Background: Much interest has been generated recently by both fatty acid amide hydrolase (FAAH) and its inhibitors as the role of FAAH in regulating the tone of endogenous cannabinoid signaling unfolds. Radiotracers which bind to FAAH, and which act as central biomarkers of CNS FAAH activity, would be useful tools to delineate the role of FAAH in both disease and addiction. We have synthesized, radiolabelled, and evaluated *ex vivo* in rats a variety of potent FAAH inhibitors; chiefly in the prototypical carbamate class but also the urea PF-04457845, currently undergoing clinical trials for pain management. Several analogues show promise as radiotracers for imaging FAAH by PET.
Methods: Those synthesised FAAH inhibitors which had nanomolar potency *in vitro* were radiolabelled in the carbonyl position with carbon-11 by direct $[^{11}C]CO_2$ fixation techniques (Figure) in one-pot sequences at high specific activities. Upon HPLC purification, the formulated radiotracers were administered to SD rats via tail-vein and animals sacrificed at 2 and 40 mins post-injection. Brain regions were excised and counted for radioactivity. Blocking studies to determine specificity of binding were performed by pre-treatment with the FAAH classical inhibitor URB 597. For select radiotracers, the kinetics of *in vivo* irreversible binding were determined by brain homogenization techniques.
Results: All eight of the novel and potent radiotracers were synthesized in high radiochemical purities (>97%) and with high specific activities (1500-5000 mCi/μmole). After iv injections to rats, moderate to high brain penetration was observed with SUVs from 0.8 to 4 at 40 min post injection. While there is no brain region devoid of FAAH, in all cases the FAAH-rich cortex displayed higher uptake than the FAAH-poor hypothalamus. Specific binding to FAAH represented 75-90% of total binding as determined by pre-treatment with URB 597 (2 mg/kg ip). Specific binding of the radiotracers to FAAH was irreversible as shown by brain homogenate studies but the rate of binding varied considerably.
Conclusions: Several of the novel carbon-11 radiotracers described here have considerable potential for imaging FAAH with PET. They displayed high brain uptake, appropriate regional distribution, and specificity for FAAH. Having radiotracers with a range of binding kinetics will be useful in designing the optimal radiotracer in human FAAH imaging studies.

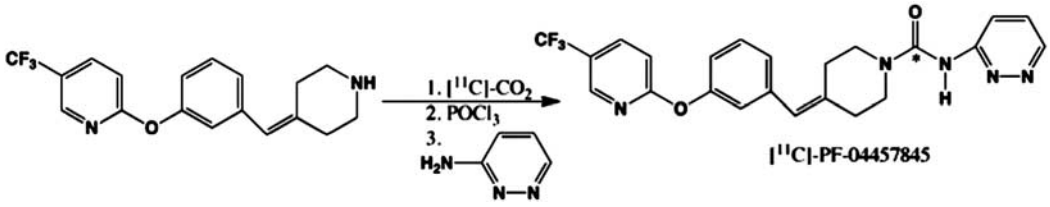

O6. Human PET imaging with [11C]JNJ-42491293, a tracer for the mGluR2 positive allosteric site

Mark Schmidt[1], Michel Koole[2], Jan De Hoon[2], Anne Van Hecken[2], Kristof Dubois[3], Jose Andres[4], Guy Bormans[2] and Koen Van Laere[2]

[1]Janssen Pharmaceutica, N.V., Belgium; [2]Catholic University of Leuven, Belgium; [3]Janssen Pharmaceutica, Belgium; [4]Janssen-Cilag, Toledo, Spain

Background: The metabotropic glutamate receptor subtype 2 (mGluR2) is widely distributed in brain including cerebral cortex, cerebellum, and subcortical structures. The receptor is predominantly presynaptic and modulates the release of glutamate through feedback inhibition. Orthosteric agonists for group 2 mGluRs have been identified and have shown beneficial effects in a variety of preclinical behavioral models and clinical conditions including anxiety and schizophrenia. Recently, positive

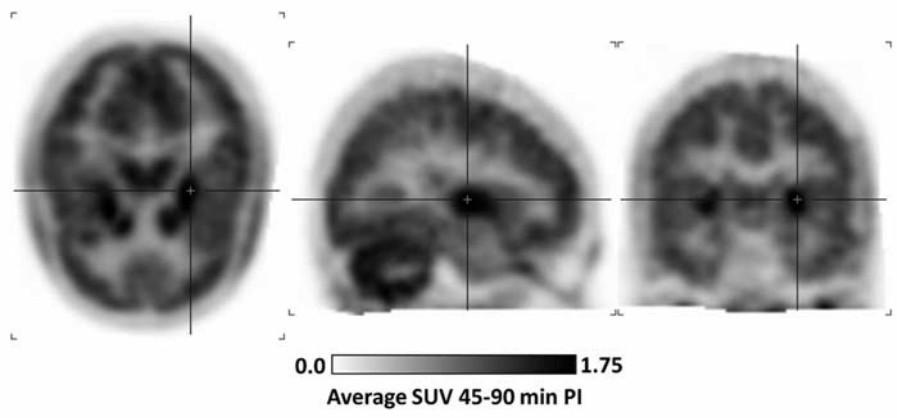

Figure Summed image of the distribution of [^{11}C]JNJ-42491293 in human brain.

allosteric modulators (PAMs) of the mGluR2 have been developed as a potentially more selective and nuanced approach to enhancing mGluR2 function. The location of the allosteric site or sites on the receptor is not known but is not identical with the agonist binding site and chemotypes for candidate mGluR2 PAMs are quite different from the scaffold typical of orthosteric ligands. [^{11}C]JNJ-42491293 has been identified as a candidate PET tracer for an mGlu2 allosteric site. Preclinical studies of [^{11}C]JNJ-42491293 indicate high affinity (IC50 = 9.6 nM) and selectivity of the tracer for the human mGluR2, and showed that *in vivo* binding is reversible and displaceable by compounds targeting this allosteric site. As such, it can be used for profiling the distribution of the mGluR2 in human *in vivo* and may be useful for testing target engagement and dose occupancy of clinical leads with affinity for the same site. The safety, biodistribution, dosimetry, and kinetic modeling of [^{11}C] JNJ-42491293 was determined in humans in preparation for possible occupancy studies.
Methods: Studies were conducted in 20 healthy male subjects (age range 19-35 y) on a Siemens HiRez 16 slice LSO PET/CT camera. Biodistribution and radiation burden was determined in the first 3 subjects using dynamic whole-body PET-CT. Effective doses were calculated with OLINDA based on image-derived source organ residence times. Dynamic brain scans were acquired over 90 minutes from time of injection in the subsequent 17 healthy volunteers along with arterial and venous sampling and metabolite determination. Regional tissue distribution and tissue and blood kinetics of the tracer were analyzed using PMOD. Safety and tolerability were assessed.
Results: [^{11}C]JNJ-42491293 was readily taken up in the brain, with maximum activity around 30 minutes in grey matter followed by uniform decline. Retention in grey matter relative to white matter was similar throughout cortex, and was higher in striatum and cerebellum, consistent with reported distribution of the mGluR2 in brain. The tracer appeared to be retained in striate muscle including the heart, consistent with the reported expression profile for mGluR2. The effective radiation dose was 4.2 microSv/MBq. [^{11}C]JNJ-42491293 dynamic profiles could be fitted to a 2 tissue compartment model. Arterial and venous intact tracer fractions were very similar ($R^2 = 0.944$) with 30% present after 90 minutes. Volume of distribution (V_T) was between 3 and 7 ml.cm^{-3} for cortex, subcortical grey matter and cerebellum. No serious adverse events occurred; adverse events were mild and generally related to experimental procedures.
Conclusions: These results support [^{11}C]JNJ-42491293 as a PET tracer for measuring mGluR2 availability in humans that may be suitable for assessment of occupancy by mGluR2 PAM drug candidates.

O7. A novel PET radiotracer for imaging the kappa opioid receptor

Ming-Qiang Zheng[1], Daniel Holden[1], Shu-Fei Lin[1], Charlie Mitch[2], Antonio Navarro[2], Vanessa Barth[2], Steve Quimby[2], Jim Ropchan[1], Richard E. Carson[1] and Yiyun Huang[1]

[1]PET Center, Yale University, New Haven, Connecticut; [2]Eli Lilly & Co., Indianapolis, Indiana, USA

Background: Multiple lines of evidence have demonstrated the involvement of the kappa opioid receptor (KOR) in psychiatric disorders such as anxiety, depression, drug abuse and alcoholism. The goal of this study was to synthesize the selective KOR antagonist [^{11}C]F3PB {[^{11}C]4-(4-(((*S*)-2-(pyridin-3-yl)-pyrrolidin-1-yl)methyl) phe-noxy)-3-fluorobenzamide}, and evaluate its potential as a new PET imaging tracer.
Methods: [^{11}C]F3PB was prepared by cyanation of the iodophenyl precursor followed by hydrolysis of the benzonitrile intermediate to an amide. PET

imaging studies were performed in rhesus monkeys using the Focus-220 scanner. Arterial input functions were generated for each scan. Metabolite analysis was performed with HPLC. Plasma free fraction was determined by ultrafiltration. Imaging data were analyzed with compartment models and the simplified reference tissue model (SRTM) with cerebellum as reference.

Results: F3PB displayed high *in vitro* binding affinity and selectivity for the kappa opioid receptor. (Ki of 0.18, 7.68, and 91.3 nM, respectively, for κ, μ, and δ receptor). [^{11}C]F3PB was prepared in >95% radiochemical purity and mean radiochemical yield of 10.7% (EOS, n = 7). [^{11}C]F3PB was metabolized fairly quickly. At 30 min following tracer injection, parent fraction in the plasma was ~20%. Plasma free fraction was 4.3 ± 0.4% (n = 7). In the monkey brain, it displayed fast uptake kinetics, with regional activity peaked at ~10 min post-injection. Regional time-activity curves were well described with the 2-tissue compartment model and SRTM. Mean regional binding potential (BP_{ND}) values from SRTM analysis were 2.15, 1.32, 1.07, 1.05, and 0,6, respectively, for the globus pallidus, cingulate cortex, putamen, caudate and frontal cortex (n = 3). Specific binding was completely blocked by pretreatment with naloxone (1 mg/kg, iv, n = 2) and dose-dependently by the selective KOR antagonist LY2456302 (various dose).

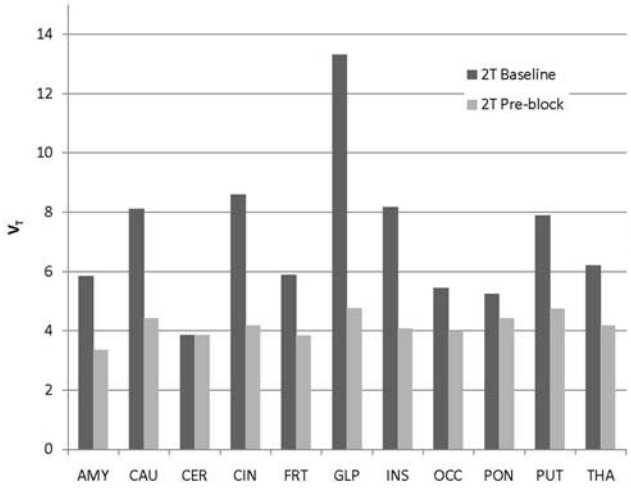

Figure 2T V_T of [^{11}C] F3PB in selected ROIs of monkey brain at Baseline and 1 mg/kg Naloxona Pretreatment (AMY: amygdala, CAU: caudate, CER: cerebellum, CIN: cingulate, FRT: frontal cortex, GLP: globus pallidus, INS: insula, OCC: occipital cortex, PUT: putamen, THA: thalamus).

Conclusions: [^{11}C]F3PB demonstrates favorable properties as a PET radiotracer for *in vivo* imaging of the kappa opioid receptor. An added advantage of this tracer is that it can be labeled with the longer-lived isotope F-18, whose preparation and evaluation is currently underway.

O8. [^{11}C]Elacridar, a PET radiotracer to measure the function of P-glycoprotein and breast cancer resistance protein at the blood-brain barrier: first assessment in healthy human subjects

Martin Bauer[1], Markus Zeitlinger[1], Cecile Philippe[2], Johann Stanek[1,3], Georg Dobrozemsky[2], Wolfgang Wadsak[2], Markus Mitterhauser[2], Georgios Karanikas[2], Markus Müller[1] and Oliver Langer[1,3]

[1]Department of Clinical Pharmacology, Medical University of Vienna, Austria; [2]Department of Nuclear Medicine, Medical University of Vienna, Austria; [3]Health and Environment Department, AIT Austrian Institute of Technology GmbH, Seibersdorf, Austria

Background: The multidrug efflux transporters P-glycoprotein (Pgp) and breast cancer resistance protein (BCRP) form a concerted defence mechanism at the blood-brain barrier (BBB) where they restrict the brain distribution of several clinically used drugs. Animal studies have demonstrated that [^{11}C]elacridar is a dual substrate of Pgp and BCRP, which shows a low degree of *in vivo* metabolism and which lacks brain uptake of radiolabeled metabolites.[1] The aim of this study was to perform an initial evaluation of [^{11}C]elacridar in healthy humans subjects as a potential PET radiotracer to measure Pgp and BCRP function at the human BBB.

Methods: In 4 healthy subjects dynamic [^{11}C]elacridar brain PET scans and arterial blood sampling were performed over 120 min. At 60 min after injection of

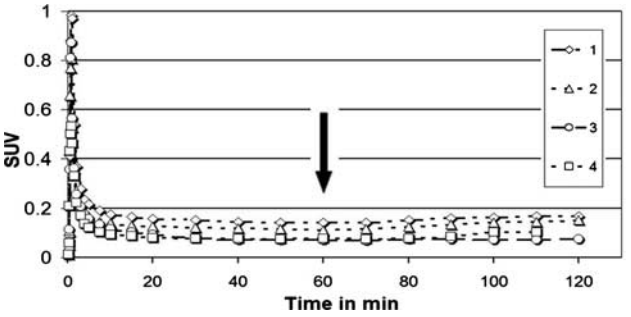

Figure 1 Whole brain grey matter time-activity curves of [^{11}C]elacridar expressed as SUV in 4 healthy volunteers. The Pgp inhibitor tariquidar was infused from 60 to 90 min after radiotracer injection (start of infusion indicated by arrow) at a dose of 3 mg/kg body weight.

[^{11}C]elacridar, subjects received an i.v. infusion of the potent Pgp inhibitor tariquidar (AzaTrius Pharmaceuticals Pvt. Ltd., London, UK) at a dose of 3 mg/kg body weight over 30 min. Radiolabeled metabolites of [^{11}C]elacridar in plasma were measured with a solid-phase extraction/HPLC assay. Brain activity uptake was expressed as the ratio of the area under the whole brain grey matter time-activity curve to the area under the plasma time-activity curve from time 0 to 60 min ($AUC_{0–60\ brain}/AUC_{0–60\ plasma}$). In 4 additional subjects whole body PET/CT scans were acquired over 100 min.

Results: Brain activity uptake was low after injection of [^{11}C]elacridar with a mean $AUC_{0–60\ brain}/AUC_{0–60\ plasma}$ of 0.13 ± 0.03. No change in whole brain time-activity curves was observed during or after tariquidar infusion (Figure 1). At 60 min after radiotracer injection, $86 \pm 5\%$ of total radioactivity in arterial plasma was in the form of unchanged parent radiotracer. Whole body scans showed that [^{11}C]elacridar was mainly excreted *via* the hepatobiliary route. The estimated total effective dose was 2.8 μSv/MBq.

Conclusions: Low brain uptake in humans was consistent with [^{11}C]elacridar being a dual substrate of Pgp and BCRP. In a previous human PET study with the Pgp substrate radiotracer (*R*)-[^{11}C]verapamil we have observed a pronounced increase in brain time-activity curves in response to tariquidar infusion.[2] This effect was not observed in the present study with [^{11}C]elacridar, in all likelihood because tariquidar preferentially blocked Pgp at the studied dose and [^{11}C]elacridar was still actively effluxed by BCRP at the BBB. [^{11}C]Elacridar may be a useful radiotracer to study Pgp and BCRP function at the human BBB.

Acknowledgements: The research leading to these results has received funding from the European Community's Seventh Framework Program under grant agreement 201380 (Euripides) and from the Austrian Science Fund (FWF) project ''Transmembrane Transporters in Health and Disease'' (SFB F35).

References

[1] Dörner B et al. *J Med Chem* 2009; 52(19):6073-82.
[2] Wagner CC et al. *J Nucl Med* 2009; 50(12):1954-61.

O9. Validation of SUV as an outcome measure of [^{11}C]PBR28 in rat using PET/MRI

Janine Doorduin[1,2], Jenny Häggkvist[1], Miklós Tóth[1], Kálmán Nagy[1], Andrea Varrone[1], Domokos Máthé[3], Christer Halldin[1] and Balázs Gulyás[1]

[1]Karolinska Institutet, Department of Clinical Neuroscience, Stockholm, Sweden; [2]University Medical Center Groningen, Department of Nuclear Medicine and Molecular Imaging, Groningen, The Netherlands; [3]CROmed Ltd, Budapest, Hungary

Background: To increase our understanding of the role of microglia in neurological disorders animal models are of great value. Small animal PET allows for studying microglia activation in these models longitudinally, using radioligands that bind to the translocator protein (TSPO). There are however methodological challenges for quantification of this receptor and, consequently, microglia activation. There is no suitable reference region and the use of plasma-derived input is not an option for longitudinal studies. The aim of this study was therefore to evaluate the use of the semi-quantitative standardized uptake value (SUV) as an outcome measure in small animal PET studies on microglia activation for the TSPO ligand [^{11}C]PBR28 [1]. In addition, the test-retest variability of the SUV was determined.

Methods: Healthy male Wistar rats (n = 8, 363 ± 57 grams) were divided in two groups. The first group (n = 4) was used to determine the correlation between the distribution volume (V_T) obtained by Logan graphical analysis and the SUV (t = 57-63 min after injection). In the second group (n = 4) the test-retest variability of the SUV (t = 57-63 min) was determined, with a 7-day interval between scans.

Dynamic PET scans of 63 minutes were acquired after injection of 23 ± 5 MBq [^{11}C]PBR28, with the nanoScan® PET/MRI (Mediso Ltd, Budapest, Hungary [2]). An MRI scan was made for anatomical reference. For the first group arterial blood samples (n = 16) were taken during the scan for radioactivity measurements in blood and plasma, as well as radiometabolite analysis (n = 3).

Results: The brain uptake of [^{11}C]PBR28 was highest at 1 minute after injection and reached a steady state at 45 minutes. [^{11}C]PBR28 in blood and plasma peaked at 10-15 seconds after injection. Radiometabolite analysis showed that at 4 minutes after injection 43 ± 10% of the total radioactivity in plasma was [^{11}C]PBR28, which was reduced to 4 ± 3% at 60 minutes. The time-activity curves of 9 different regions were fitted with Logan graphical analysis, using radiometabolite corrected plasma input. The whole brain V_T was 43.1 ± 1.2. The highest V_T was found in the cerebellum (54.0 ± 1.9), whereas the thalamus had the lowest V_T (34.2 ± 2.7). A statistical significant correlation

($r^2 = 0.95$; $p < 0.0001$) was found between the V_T and the SUV (0.63 ± 0.05 for whole brain). The whole brain uptake of [^{11}C]PBR28 in the test-retest study (average SUV 0.49 ± 0.07) showed an intersubject variability of 14.3% and a retest variability of 13.6%. The interclass correlation coefficient (ICC) was 0.59, showing that the variability is higher between than within rats. Similar or higher ICC values (0.58-0.88) were found for the other brain areas, with exception of the cortex (0.33).

Conclusions: The SUV of [^{11}C]PBR28 showed a high correlation with the V_T as obtained by Logan graphical analysis, as well as a good test-retest variability. For future longitudinal small animal PET studies the SUV can thus be used to describe [^{11}C]PBR28 uptake in healthy brain tissue.

References

[1] Imaizumi M et al. *Neuroimage* 2008; 39(3):1289-98.
[2] Nagy N et al. *J Nucl Med* 2011; 52(suppl 1):259.

O10. Correcting for the Ala147Thr polymorphism in the gene for 18 kDa translocator protein improves quantification of this inflammatory biomarker with [^{11}C]PBR28

William Kreisl[1], Kimberly Jenko[1], Christina Hines[1], Chul Hyoung Lyoo[1], Cheryl Morse[1], Sami Zoghbi[1], Joel Kleinman[2], Victor Pike[1], Francis McMahon[3] and Robert Innis[1]

[1]Molecular Imaging Branch; [2]Clinical Brain Disorders Branch; [3]Human Genetics Branch, National Institute of Mental Health, National Institutes of Health, Bethesda, Maryland, USA

Background: The second generation radioligand for the 18 kDa translocator protein (TSPO), [^{11}C]PBR28, has greater specific-to-nonspecific binding than the prototypical radioligand [^{11}C]*(R)*-PK 11195. However, TSPO shows differential affinity for [^{11}C]PBR28 and similar radioligands in human studies, likely caused by the TSPO Ala147Thr polymorphism. We sought to determine if 1) TSPO genotype correlates with PBR28 binding both *in vitro* and *in vivo*, 2) differential affinity of PBR28 exists in both control and schizophrenia brain tissue, and 3) stratifying subjects by genotype could increase statistical power of [^{11}C]PBR28 to detect group differences in TSPO density in a hypothetical clinical study.
Methods: Twenty-seven healthy volunteers (age 46 ± 18 years, 11 female) underwent [^{11}C]PBR28 imaging. Total [^{11}C]PBR28 binding (V_T) was calculated with the two-tissue compartment method using the arterial input function. Peripheral lymphocytes from these subjects were used to perform binding assays with [^{3}H]PK 11195 and increasing concentrations of nonlabeled PBR28. Specific binding of [^{3}H]PBR28 was measured *in vitro* from dorsolateral prefrontal cortex (DLPFC) homogenates from additional healthy controls ($n = 37$) and patients with schizophrenia ($n = 37$). All subjects were genotyped for the Ala147Thr polymorphism and categorized as HH, HL, or LL depending on the presence of the polymorphism on neither, one, or both TSPO alleles. Measured [^{3}H]PBR28 specific binding in DLPFC (*in vitro* study) and measured ratio of V_T between HH and HL volunteers (*in vivo* study) was used to estimate total [^{11}C]PBR28 binding in healthy controls and schizophrenia patients.
Results: Binding assays showed 100% agreement with genotype assay, with HH subjects fitting a one-site model and HL subjects fitting a two-site model, indicative of two different affinity states of TSPO present in lymphocytes of HL subjects. HH subjects had 35–55% greater [^{11}C]PBR28 binding than HL subjects in all regions measured (frontal, parietal, occipital, temporal, medial temporal, and cingulate cortex, $p < 0.02$, unpaired t test, FDR corrected). HH, HL, and LL subjects were identified with similar frequencies in both control and schizophrenia cohorts, with specific binding of [^{3}H]PBR28 highest in HH subjects, lowest in LL subjects, and intermediate in HL subjects for both controls and patients. Schizophrenia patients had greater specific binding than controls in each genotype group ($p < 0.001$). The estimated effect size for difference in [^{11}C]PBR28 binding between schizophrenia patients and controls increased after stratifying subjects into HH and HL groups (1.7 *vs.* 2.3 and 1.9, respectively).
Conclusions: The Ala147Thr polymorphism is associated with reduced *in vivo* binding with [^{11}C]PBR28. Binding assay accurately predicts TSPO Ala147Thr polymorphism status and may be used as an alternative to genotyping. Controlling for affinity status should not only allow accurate quantification of PET data, but also increase statistical power of clinical studies using [^{11}C]PBR28.

O11. [^{18}F]PBR111 binding in multiple sclerosis: relationship to age and clinical variables

Alessandro Colasanti[1], Qi Guo [1], Mayca Onega[2], Paolo Giannetti[1], Charlotte Thomas[1], Paola Piccini[1], Paul M. Matthews [1,3], Roger N. Gunn[1,2] and E.A. Rabiner[1,2]

[1]Imperial College London, UK; [2]Imanova Ltd, London, UK; [3]GlaxoSmithKline, London, UK

Background: The mitochondrial protein TSPO is overexpressed on activated microglia. PET imaging with TSPO radioligands has been applied in a variety of neurological conditions, including Multiple Sclerosis (MS), to visualize *in vivo* the activation of microglia in the diseased brain. [^{18}F]PBR111 is a 2nd generation TSPO PET tracer with promising pre-clinical characteristics, which has not been tested in humans to date. We aimed to characterize the binding of [^{18}F]PBR111, in the brain of MS patients and healthy subjects, and explore the relationship of binding to clinical-demographic variables and impairment of cognitive functioning.
Methods: Age- and gender- matched MS patients and healthy volunteers ($n=8$ per group, all females, aged 48.1 ± 7.5 and 47.5 ± 10.2 years, respectively) underwent a PET scan with [^{18}F]PBR111. The regional total volume of distribution (V_T) was quantified using the 2 tissue compartment model, and a metabolite corrected plasma input function. As caudate V_T was the lowest across the whole brain, we derived a pseudo-binding potential using the gray matter masked caudate ($BP_{REF}=V_T^{ROI}/V_T^{caudate}-1$) as a reference region to explore outcome measures independent of plasma variability. Regions of interests (ROIs) included the whole cortical and subcortical grey matter, the whole white matter, neocortical regions, cingulate cortex, insula, hippocampus, cerebellum, thalamus, brainstem regions, and corpus callosum. Clinical characterization included disability (EDSS scores) and number of recent relapses. Tests of attention, visuo-spatial ability, executive functioning, logic, working, and semantic memory were performed using the Rey-Osterrieth complex figure (ROCF), the Trail-Making Tests (TMT A&B), the Wechsler Logic Memory (WLM), the Verbal Fluency (VF) and the Digit Span (DS) tests.
Results: We found a high inter-individual variability of [^{18}F]PBR111 BP_{REF} both in MS patients and healthy volunteers in all ROIs ($c_v=42.7\%$). Across the whole study population, age was positively correlated with [^{18}F]PBR111 BP_{REF} ($r>0.5$; $p<0.01$) in all the ROIs except the neocortical regions, pons, medulla, and corpus callosum. Examining the healthy volunteers group only, the correlation of age with [^{18}F]PBR111 BP_{REF} remained significant ($r>0.64$, $p<0.05$) in all ROIs except the neocortical regions and corpus callosum. In MS patients EDSS scores were positively associated with [^{18}F]PBR111 BP_{REF} in the hippocampus and cerebellum ($r>0.7$, $p<0.05$, controlling for age). We observed negative correlations between ROCF recall scores and [^{18}F]PBR111 BP_{REF} in most of the neocortical regions, hippocampus, cingulate cortex and cerebellum, and between WLM delayed recall scores and [^{18}F]PBR111 BP_{REF} in all cortical regions and thalamus, while there was a positive relationship between time-to-completion TMT-A scores and binding in hippocampus and cerebellum, indicating a relationship between cognitive impairment and brain TSPO density. These results were significant after controlling for age.
Conclusions: We found high inter-individual variability of [^{18}F]PBR111 binding. In most ROIs [^{18}F]PBR111 binding was highly correlated with age, consistent with previous observations using other TSPO tracers. Furthermore, despite the limited number of subjects we could observe that higher [^{18}F]PBR111 binding was associated with higher severity of disease and poorer cognitive performance in MS patients.

O12. Imaging activated microglia in Parkinson's disease: a PET study with a novel radiotracer, [^{18}F]FEPPA

Ji Hyun Ko[1,2], Y. Koshimori[1,2], R. Mizrahi[1], P. Rusjan[1], A. Wilson[1], S. Houle[1], A.E. Lang[2] and A.P. Strafella[1,2]

[1]PET Imaging Centre, Centre for Addiction and Mental Health, University of Toronto, Toronto, Canada; [2]Toronto Western Hospital (Movement Disorders Centre) & Research Institute (Division of Brain, Imaging and Behaviour - Systems Neuroscience, BIB-SN), UHN, University of Toronto, Ontario, Canada

Background: It is well documented that neuroinflammation may play an important role in neurodegeneration in Parkinson's disease (PD). Post-mortem studies have confirmed the presence of reactive microglia and astrocytes. Previous PET imaging studies also reported a possible role of neuroinflammation in PD. Here, we

used a recently developed PET radioligand, [^{18}F]FEPPA, binding to the translocator protein (TSPO) to measure level of microglial activation in PD.
Methods: Nine PD patients and twelve age-matched healthy controls underwent a [^{18}F]FEPPA PET and MRI scan. Arterial plasma sampling and metabolite analysis were performed to create plasma input curves. A 2-compartment model analysis was applied and total distribution volume (V_T) was calculated in each region-of-interest (ROI) delineated by fully automated procedure. Student t-test is used to test the difference between the PD patients and controls.
Results: PD patients showed significantly higher [^{18}F]FEPPA V_T in the striatum, particularly the left putamen (PD: 11.1 ± 1.77 vs. controls: 7.45 ± 0.73; $p < 0.05$) and left caudate (PD: 9.42 ± 1.21 vs. controls: 5.46 ± 0.67; $p < 0.05$). The TSPO expression was also elevated in the thalamus (PD: 13.5 ± 1.42 vs. controls: 9.85 ± 0.94; $p < 0.05$).
Conclusions: The subcortical increase of [^{18}F]FEPPA V_T suggests that microglia activation is significantly elevated in PD. This tracer may provide a valuable *in vivo* evaluation of neuroinflammation's role in PD.

O13. Low brain CB1 receptor occupancy by a second generation CB1 antagonist TM38837 in comparison with rimonabant in nonhuman primates

Akihiro Takano[1], Balázs Gulyás[1], Katarina Varnas[1], Paul Brian Little[2], Pia K. Norregaard[2], Niels Ole Jensen[2], Christian E. Elling[2] and Christer Halldin[1]

[1]Karolinska Institutet, Department of Clinical Neuroscience, Center for Psychiatric Research and Education, Sweden; [2]7TM Pharma A/S, Denmark

Background: The endocannabinoid system plays a pivotal role, through the CB1 receptor, in regulating food intake and energy expenditure. It has been shown that CB1 receptor antagonists/inverse agonists not only inhibit food intake and reduce body weight in animals and humans but also directly modulate fat metabolism at peripheral sites in skeletal muscle, adipose tissue, and the liver. Although the first generation CB1 antagonists such as rimonabant and taranabant showed clinical efficacy, they showed severe CNS side effects such as anxiety, depression and suicidal ideation. To eradicate such CNS side effects, compounds with a profile of restriction to peripheral CB1 receptors have been developed. In this PET study, we investigated the brain CB1 receptor occupancy of a second generation CB1 receptor antagonist TM38837 in comparison with rimonabant in nonhuman primates. An autoradiographic blocking study was also performed using postmortem human and non human primate brains.
Methods: Two cynomolgus monkeys were used in the PET study. PET measurements were performed for 120 min with High Resolution Research Tomograph (HRRT) (Siemens) after injection of [^{11}C]MePPEP at baseline and at pretreatment conditions. Pretreatment was by intravenous administration at dose levels of 0.3-4.0 mg/kg of bolus injection and 3.0 mg/kg of bolus plus 3.0 mg/kg/hr of infusion for TM38837 and 0.3-3.0 mg/kg of bolus injection for rimonabant. Brain CB1 receptor binding was calculated using average SUV at late time based on the previous quantitative report [1]. Brain CB1 receptor occupancy was calculated with the difference of SUV values at baseline and at pretreatment conditions using Lassen plot. Relationship between brain CB1 receptor occupancy and dose/plasma concentration were evaluated with hyperbolic functions. Kd values, at which 50% of CB1 receptor was occupied, were calculated. In the autoradiography study, the blocking effect to [^{125}I]SD7015 accumulation by TM38837 (10 μM) and rimoabant (10 μM) was evaluated using postmortem human and non-human primate brain slices.
Results: CB1 receptor occupancy by both TM38837 and rimonabant increased in a dose/plasma concentration dependent manner. However, Kd values for dose was found to be approximately 10 times higher in TM38837, and Kd values for plasma concentration was found to be more than 100 times higher for TM38837, which indicated much lower CNS penetration of TM38837. In autoradiography study, [^{125}I]SD7015 accumulation was blocked by both TM38837 and rimonabant, which indicated that both have high affinity to CB1 receptor.
Conclusions: Only low levels of brain CB1 receptor was demonstrated to be occupied by TM38837 although TM38837 has high affinity to CB1 receptor. This low CNS penetration of TM38837 could lead to low incidences of CNS side effects at clinical situations. The present study warrants further development to clinical application.

Reference

1. Terry GE, Liow JS, Zoghbi SS, Hirvonen J, Farris AG, Lerner A, Tauscher JT, Schaus JM, Phebus L, Felder CC, Morse CL, Hong JS, Pike VW, Halldin C, Innis RB. Quantitation of cannabinoid CB1 receptors in healthy human brain using positron emission tomography and an inverse agonist radioligand. *Neuroimage* 2009; 48:362-70.

O14. The use of [^{11}C]OMAR and positron emission tomography to investigate the pathophysiology of posttraumatic stress disorder

Christopher Bailey[1], Marc Normandin[2], Shannan Henry[3], Allison Greene[4], Marc Potenza[3], Richard Carson[3], Yiyun Huang[3] and Alexander Neumeister[4]

[1]Johns Hopkins University School of Medicine, Baltimore, Maryland, USA; [2]McLean Hospital, Belmont, Massachusetts, USA; [3]Yale School of Medicine, New Haven, Connecticut, USA; [4]New York University School of Medicine, New York, USA

Background: Recent preclinical and clinical evidence suggests that disruptions in CB1 receptor-mediated endocannabinoid (eCB) signaling may contribute to the neurobehavioral changes initiated by trauma exposure, and prohibit proper extinction of aversive memories in a cortico-limbic-striatal circuit that has been implicated in posttraumatic stress disorder (PTSD). The recent development of the CB1 receptor selective radiotracer, designated [^{11}C]OMAR now makes it possible for the first time to conduct an *in vivo* assessment of CB1 receptor density in PTSD using positron emission tomography (PET).
Methods: Using [^{11}C]OMAR and PET on a high resolution research tomograph (HRRT) PET scanner, we determined volume of distribution (VT) values, a measure of CB1 receptor density, under resting conditions in medication-free PTSD patients (N = 16/8F, age, ys 30.0 ± 8.5, range 20-44, CAPS 78 ± 11.5), individually-matched healthy control subjects (N = 16/8F, age, ys 30.6 ± 7.5, range 20-45). Following a transmission scan, [^{11}C]OMAR was injected over one min and HRRT list mode data was acquired for 120 minutes. Dynamic scan data was reconstructed with the following corrections: attenuation, normalization, scatter, randoms, and deadtime. Motion correction of PET data was performed via frame-by-frame registration to a summed image (0-10 min post injection). A new summed image was then created from the motion-corrected data and registered to the participant's T1-weighted MR images, which, in turn, were registered to an MR template. Gray matter regions of interest are taken from the template (Anatomical Automatic Labeling (AAL) for SPM2) and applied to the PET data to produce time-activity curves for relevant regions of interest (ROI) and control regions. Arterial plasma input functions were measured and a range of analysis methods were used to estimate volume of distribution (VT) from regional time activity curves (TACs). Blocking studies using unlabeled OMAR in non-human primates show that in animals the specific binding component is about 1-1.5 relative to the non-specific binding component. Assuming there is no species difference we assume that this ratio is the same in our population. Data were analyzed using linear mixed models with [^{11}C]OMAR VT as the dependent variable, region (Amygdala, Hippocampus, Anterior Cingulate, Posterior Cingulate, Caudate, Putamen, Pallidum) as within-subject factor and diagnosis and gender as between-subject factors.
Results: We found elevated CB1 binding in PTSD relative to the healthy control subjects in all regions of the aforementioned PTSD circuit ($F(1,28) = 12$, $p < .0017$) (Percent Difference PTSD vs HC, Amygdala: 29.6, ACC: 25.6, PCC: 26.1, caudate: 27.6, hippocampus: 26.2, pallidum: 31.1, putamen: 24.4). Independent of diagnosis, we found significantly higher CB1 binding in women relative to men ($F(1,28) = 9.88$, $p < .0039$).
Conclusions: Our data show that the maladaptive neurobehavioral trauma response in PTSD is associated with impaired eCB signaling as evidenced by upregulation of CB1 receptors. In addition, we found evidence for gender differences in CB1 receptor denisty in both PTSD and healthy people.

O15. Mapping CB_1 cannabinoid receptors with [^{3}H]OMAR in the Flinders rodent model of depression

Adjmal Nahimi[1,2], Albert Gjedde[3], Dean F. Wong[1,2,3], Tomas R. Guilarte[4], Jennifer Dziedzic[4], Heather Valentine[3], Jongho Kim[3], Andrew Horti[3] and Wegener Gregers[5]

[1]Department of Nuclear Medicine and PET Centre, Aarhus University Hospitals, Aarhus University, Denmark; [2]Department of Neuroscience and Pharmacology, University of Copenhagen, Denmark; [3]Department of Radiology and Radiological Science, Division of Nuclear Medicine, Johns Hopkins Medical Institutions, Baltimore, MD, [4]Department of Environmental Health Sciences, Mailman School of Public Health, Columbia University, [5]Centre for Psychiatric Research, Aarhus University Hospitals, Aarhus University, Denmark

Background: The endocannabinoid system regulates cognitive and emotional processes and pathology of this system is implicated in psychiatric disorders, including depression and schizophrenia. The precise

role of the endocannabinoid system in psychiatric disorders remains unclear, but changes in expression of CB_1 receptors and subsequent altered modulation of monoamines is suggested in depression (Esteban & García-Sevilla, 2011). CB_1 receptor agonists, such as WIN55,212-2 and CP55,940 regulate synthesis and release of monoamines and are suggested as a novel therapy in the treatment of depression. However, further studies are needed to identify the precise mechanisms of action and pathology of the endocannabinoid system in depression. The hypothesis that depressive-like traits are related to altered CB_1 receptor expression were tested in *in-vitro* autoradiography experiments, measuring binding of [^{3}H]OMAR, a highly selective CB_1 receptor antagonist (Horti et al, 2006) in the Flinders rodent model of depression.

Methods: The Flinders sensitive line (FSL) (N = 5-6) was used as a model of depression and the Flinders resistant line (FRL) (N = 6-8) served as controls (Wegener et al. 2010). In these rats, CB_1 receptor autoradiography in postmortem tissue was carried out by incubating 20 μM thick sagital sections in the presence of the CB_1 receptor antagonist [^{3}H] OMAR (method adapted from Mato & Pazos 2004, with small modifications). Non-specific binding was determined on adjacent sections in the presence of [^{3}H]OMAR and the CB receptor agonist CP55,940.

Results: Eighteen regions of interest were analyzed on the autoradiogram. The highest binding (in units of pmol/g ± SD) was found in the hippocampus (105 ± 21 in FSL and 105 ± 16 in FRL), striatum (69 ± 20 in FSL and 75 ± 17 in FRL), cerebellum (121 ± 40 in FSL and 111 ± 17 in FRL), and cortex (51 ± 13 in FSL and 53 ± 7 in FRL) (see Figure 1). In refutation of the hypothesis, these estimates of [^{3}H]OMAR binding in FSL and FRL rats were not significantly different.

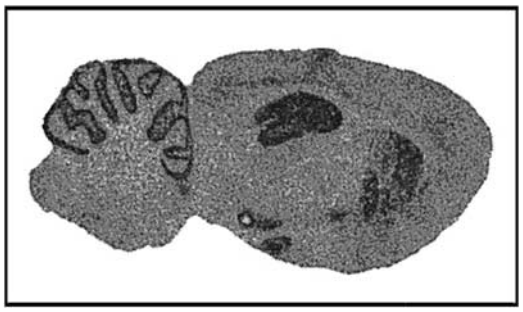

Figure 1 Image of [^{3}H] OMAR binding to CB_1 receptors in the Flinders rodent model of depression (see text for detail).

Conclusions: Although changes in CB_1 receptor expression have been demonstrated in human suicide victims with depression and in animal models of depression, the present maps of [^{3}H]OMAR binding revealed no difference between FSL and FRL rats. We used a single concentration of [^{3}H]OMAR in this study. In future studies with several concentrations of [^{3}H]OMAR, we will test the hypothesis that depression-like behavior of FSL rats is related to changes of the kinetic Michaelis constants K_d and B_{max} of CB_1 binding.

References

Esteban, S, García-Sevilla, JA (2011), *Progress in Neuro-Psychopharmacology & Biological Psychiatry*; doi:10.1016/j.pnpbp.2011.11.007.

Horti, AG et al. (2006), *Journal of Nuclear Medicine* 47(10), 1689–1696.

Mato, S, Pazos, A (2004), *Neuropharmacology* 46(5): 716–726; doi:10.1016/j.neuropharm.2003.11.004.

Wegener G et al. (2012), *Curr Top Behav Neurosci*; doi: 10.1007/7854_2011_192.

O16. Reduced cannabinoid CB_1 receptor binding in alcohol dependence measured with positron emission tomography

Jussi Hirvonen[1], Paolo Zanotti-Fregonara[1], John C. Umhau[2], David T. George[2], Denise Rallis-Frutos[1], Chul Hyoung Lyoo[1], Cheng-Ta Li[1], Christina S. Hines[1], Hui Sun[2], Garth E. Terry[1], Cheryl Morse[1], Sami S. Zoghbi[1], Victor W. Pike[1], Robert B. Innis[1] and Markus Heilig[2]

[1]Molecular Imaging Branch, National Institute of Mental Health, NIH, Bethesda, Maryland, USA; [2]Laboratory of Clinical and Translational Studies, National Institute on Alcohol Abuse and Alcoholism, NIH, Bethesda, Maryland

Background: Brain cannabinoid CB_1 receptors contribute to alcohol-related behaviors in experimental animals. Chronic alcohol exposure decreases the density of CB_1 receptors in rodents, and a postmortem study recently found decreased CB_1 receptor density in the ventral striatum of human patients with alcohol dependence. A common single nucleotide polymorphism in the CB_1 receptor gene, *rs2023239*, is associated with alcohol dependence in the population and higher density of CB_1 receptor *in vitro*. Whether cannabinoid CB_1 receptors are decreased *in vivo* in human subjects with alcohol dependence and whether *rs2023239* modulates CB_1 receptors *in vivo* is unknown.

Methods: We measured CB_1 receptors in alcohol dependent patients (aged 44 ± 10 years, 5–50 years of

alcohol use) in early and protracted abstinence, and in comparison with control subjects with no alcohol-use disorders (aged 44 ± 10 years). We used positron emission tomography (PET) and [^{18}F]FMPEP-d_2, a radioligand for CB_1 receptors. We scanned 18 male inpatients with alcohol dependence twice, within 3–7 days of admission from ongoing drinking, and after 2–4 weeks of supervised abstinence. Imaging data were compared with those from 19 age-matched healthy male subjects without alcohol use disorders. Data were also analyzed for potential influence of the common functional variation *rs2023239* in the CB_1 receptor gene. Arterial blood was sampled during PET scans to estimate receptor binding as distribution volume (V_T), which is the ratio at equilibrium of the concentration of radioactivity in brain to that of the parent radioligand in plasma.

Results: On the first scan, V_T of [^{18}F]FMPEP-d_2 was 20–30% lower in patients with alcohol dependence than in control subjects in all brain regions and was negatively correlated with years of alcohol abuse but not with measures of withdrawal or craving. This decrease was not confounded by cigarette smoking. The plasma free fraction of [^{18}F]FMPEP-d_2 was not lower in patients with alcohol dependence (0.4 ± 0.1%) than in healthy subjects (0.4 ± 0.2%), and therefore did not cause reduction in V_T. After 2–4 weeks of abstinence, V_T of [^{18}F]FMPEP-d_2 did not change and, thus, remained similarly reduced in these patients. Irrespective of diagnostic status, *C* allele carriers at *rs2023239* had higher V_T compared to non-carriers, consistent with a previous *in vitro* study.

Conclusions: Alcohol dependence is associated with a widespread reduction of cannabinoid CB_1 receptor binding in the human brain and this reduction persists at least 2–4 weeks into abstinence. The correlation of reduced binding with years of alcohol use suggests an involvement of CB_1 receptors in alcohol dependence in humans. In a direct *in vivo* correlate of *in vitro* ligand binding data, carriers of the *C* allele of the *rs2023239* variant had higher CB_1 binding than non-carriers.

O17. PET imaging of the excitatory amino acid transporter 2 in an amyotrophic lateral sclerosis rat model

John Gerdes[1], Richard Bridges[1], Michael Braden[1], Syed Ahmed[1], Sarj Patel[1], Henry Vanbrocklin[2], Shorouk Dannoon[2], Jeffery Rothstein[3] and Rita Sattler[3]

[1]Biomedical & Pharmaceutical Sciences, University of Montana, Missoula, Montana, USA; [2]Radiology & Biomedical Imaging, University of California, San Francisco, California, USA; [3]Neurology & Brain Science Institute, Johns Hopkins University, Baltimore, Maryland, USA

Background: Excitatory amino acid transporter 2 (EAAT2) found on CNS astrocytes is the primary mechanism for clearance of extracellular levels of L-glutamate (L-Glu). Excitotoxic injury promoted by elevated L-Glu can be a result from altered regional EAAT2 activity and/or cell surface expression. Amyotrophic lateral sclerosis (ALS) is a neurodegenerative disorder marked by the progressive loss of motor neurons in the spinal cord, brain stem and motor cortex. Excessive L-Glu levels and decreased EAAT2 profiles constitute a mechanism that contributes to neuronal loss (1). ALS postmortem CNS tissue studies of L-Glu uptake into synaptosomes have revealed EAAT2 is markedly reduced. Similar focal EAAT2 losses are found in CNS tissues taken from a superoxide dismutase1 (SOD1) G93A mutant rat model that presents ALS-like symptoms and pathology (1–3). We have identified a novel EAAT2 fluorine-18 PET imaging prodrug tracer, 1, that undergoes CNS hydrolysis affording the high EAAT2 affinity radioligand 2 the capability of detecting EAAT2 in wild type (WT) rats by microPET imaging. We posit that regional CNS PET imaging of EAAT2 will quantify regional alterations in EAAT2 in ALS. To initially test this hypothesis we used tracer 1 and performed a comparative longitudinal evaluation of G93A SOD1 rats relative to WT subjects.

Methods: A G93A rat cohort was established in parallel to littermate WT controls. A cohort portion (n = 3) underwent PET imaging at three progressive times occurring from symptom onset through late stage sacrifice. An electrophilic radiosynthesis afforded tracer 1. Spine and brain PET scans were acquired with an Inveon DPET scanner, 0-90 min; i.v. tail vein. PET data were co-registered to MR scans (Bruker Biospec 7T spectrometer). The non-imaged cohort balance was sacrificed per the scans days, and then brain and spine tissues were collected for *ex vivo* analyses.

Results: Administration of 1 (> 95% purity; mean SA 2.3 Ci/mmol, n = 20) resulted in high radioactivity uptake in spine (lumbar) and brain (thalamus, cortex, and other ROIs) consistent with known EAAT2

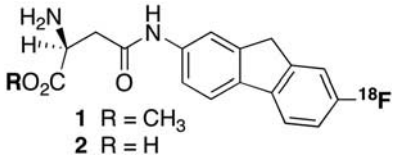

1 R = CH_3
2 R = H

densities (1). PET imaging of the G93A mutants vs. WT controls showed significant progressive reductions of EAAT2. Mutant PET data normalized to WT profiles revealed time dependent EAAT2 decreases akin to similar longitudinal determinations made previously by others quantifying L-Glu uptake into synaptosomes prepared from rat CNS postmortem tissue (3).

Conclusions: Prodrug 1 undergoes hydrolysis to radioligand 2 in the rat CNS allowing binding to and detection of EAAT2 by microPET imaging. Progressive reductions of EAAT2 in G93A SOD1 mutants as a function of pathological development are consistent with correlated postmortem tissue blot evaluations and previously described EAAT2 changes determined by synaptosome L-Glu uptake assays. The active radioligand 2 quantitatively detects progressive CNS EAAT2 changes in the rat ALS model, warranting the further development of tracer 1.

Acknowledgements: Research support provided by The Robert Packard Center for ALS Research and the Brain Science Institute, Johns Hopkins University; P2ALS; ALS Association; and NIH grants P30-NS055022 & P20-RR01583.

References

1. Rothstein JD et al., *Ann Neurol* (1995) 38:73-84.
2. Howland DS et al., *PNAS* (2002) 99:1604–9.
3. Dunlop J et al., *J Neurosci* (2003) 23:1688-96.

O18. Metabotropic glutamate receptor 5 radioligand [^{11}C]ABP688 and *N*-acetylcysteine challenge in rhesus monkeys

Christine M. Sandiego[1], Nabeel Nabulsi[2], She-Fei Lin[2], David Labaree[2], Evan D. Morris[1,2], Kelly P. Cosgrove[2,3] and Richard E. Carson[1,2]

Yale University, New Haven, Connecticut, USA, Departments of: [1]Biomedical Engineering; [2]Diagnostic Radiology; [3]Psychiatry

Background: The ability to detect changes in receptor binding at the metabotropic glutamate receptor 5 (mGluR5) could be valuable for elucidating dysfunctional glutamate transmission associated with neuropsychiatric illnesses. A recent study performed in baboons reported a significant global decrease in binding of [^{11}C]ABP688, an mGluR5 imaging probe, after administration of *N*-acetylcysteine (NAC), a facilitator of glutamate release [1]. NAC, a precursor of cysteine, indirectly increases extrasynaptic glutamate via the cysteine-glutamate antiporter, which then stimulates metabotropic glutamate receptors to modulate synaptic glutamate neurotransmission [2,3]. The aim of our study was to replicate the aforementioned study in rhesus monkeys.

Methods: Paired scans were performed in rhesus monkeys on the Focus-220 with [^{11}C]ABP688. Each monkey (n = 3) received a baseline scan followed by a challenge scan. NAC (50 mg/kg) was infused for an hour prior to the second tracer injection. In one pair of baseline/blocking scans, [^{11}C]ABP688 was administered as a bolus/infusion (B/I, $K_{bol} = 60$ min), followed by 120-min emission acquisitions. In the other two pairs of scans, [^{11}C]ABP688 was administered as a bolus followed by 90-min emission acquisitions. Listmode data were reconstructed with FBP with all corrections (attenuation, normalization, scatter, randoms, and deadtime). Time-activity curves (TACs) were generated for regions-of-interest (ROIs), derived from a nonlinear monkey template. V_T values were computed via equilibrium analysis for the B/I scans, where $V_T = C_{ROI}/C_{Plasma}$, using the concentration (C) in the ROIs and the plasma between 30–80 min. For the bolus scans, TACs were fitted with a two-tissue compartmental model to estimate V_T. The cerebellum gray matter (CGM) was used as the reference region to compute BP_{ND}, where $BP_{ND} = V_T(ROI)/V_T(CGM)-1$. Percent change in BP_{ND} was computed as $\Delta BP_{ND} = (BP_{ND}(Post)/BP_{ND}(Baseline)-1)*100$ and was averaged across studies.

Results: NAC did not significantly decrease [^{11}C]ABP688 BP_{ND} from baseline: cingulate (-4 ± 13%), occipital (-7 ± 21%), frontal (-6 ± 13%), temporal (-2 ± 9%), caudate (-2 ± 11%), and putamen (+2 ± 26%). No significant change was observed in V_T for the CGM reference region (+3 ± 11%).

Conclusions: Changes in mGluR5 BP_{ND} were not detectable with [^{11}C]ABP688 after 50 mg/kg NAC infusion. It remains to be shown whether a larger magnitude of glutamate release would induce a measurable change in [^{11}C]ABP688 binding.

References

[1] Miyake et al., 2011. Imaging changes in glutamate transmission *in vivo* with metabotropic glutamate receptor 5 tracer [^{11}C]ABP688 and *N*-Acetylcysteine challenge. *Biol Psychiatry* 1; 69(9):822–4.
[2] Dean et al., 2011. *N*-Acetylcysteine in psychiatry: current therapeutic evidence and potential mechanisms of action. *J Psychiatry Neurosci* 36(2):72–86.
[3] Melendez et al., 2005. Regulation of extracellular glutamate in the prefrontal cortex: focus on the cystine glutamate exchanger and group 1 metabotropic glutamate receptors. *JPET* 314:139–147.

O19. Tracer kinetic modeling of [^{11}C]JNJ42491293, a PET ligand for the mGluR2 receptor in the human brain

Michel Koole[1], Guy Bormans[2], Jan De Hoon[3], Inge Derdelinckx[3], Xavier Langlois[4], Sofie Celen[2], Alfons Verbruggen[2], José Ignacio Andrés[5], Mark Schmidt[4] and Koen Van Laere[6]

[1]Nuclear medicine KU Leuven Belgium; [2]Laboratory for Radiopharmacy, KU Leuven, Belgium; [3]Center for Clinical Pharmacology, KU Leuven, Belgium; [4]Janssen Research & Development, Beerse, Belgium; [5]Janssen Research & Development, Toledo, Spain; [6]Nuclear Medicine KU Leuven, Belgium

Background: We report the kinetic analysis of [^{11}C]JNJ42491293, a PET ligand for *in vivo* imaging of mGluR2 in the human brain, binding with high-affinity (hIC50 = 9.6 nM) and reversibly to the allosteric binding site. This tracer has been developed to confirm target engagement and define exposure-occupancy relationships of clinical candidates targeting this site.

Methods: 17 male subjects (age range 19–35y) were intravenously injected with 323 + /-30 MBq [^{11}C]JNJ42491293 in bolus. Starting at injection, baseline dynamic brain PET was performed for 120 min on a Siemens Biograph Hirez 16 slice PET/CT system. Blood samples were taken during the PET scan to generate an input function and to allow metabolite analysis. A triple exponential function was fitted to the plasma data, while a Watabe function [1] was fitted to the parent fraction. Dynamic PET data were reconstructed using iterative reconstructions (5 iterations, 8 subsets, 5 mm Gaussian post filter). Images were analyzed using PMOD 3.1. An average PET image was registered to the corresponding individual MR; followed by a non-linear normalization of the MR data to a T1 weighted MR template. VOIs were predefined for cortical (orbitofrontal, frontal, parietal, temporal, hippocampus, occipital), subcortical (caudate nucleus, putamen, thalamus) and brainstem regions (pons and medulla) as well as cerebellum. TACs were generated for the different VOIs. A 2 tissue (2T) compartment model, 1 tissue (1T) compartment model and Logan graphical analysis were considered for kinetic analysis using an arterial input function corrected for metabolites. For the 1T and 2T compartment models, parameters were initially estimated for the whole brain compartment and then adjusted for each VOI. For the 2T compartment, distribution volume V_{ND} for non-specific binding was assumed constant for all cortical and subcortical regions.

Results: Distribution volumes of the 2T compartment model and Logan graphical analysis were well correlated for all regions (see Figure 1). For the 2T compartment model, total distribution volume V_T and the distribution volume for specific binding for the whole brain V_S were linearly correlated, indicating a nearly constant value for non-specific distribution volume V_{ND} of 1.16 (see Figure 2). A 1T compartment model was not better than a 2T model,

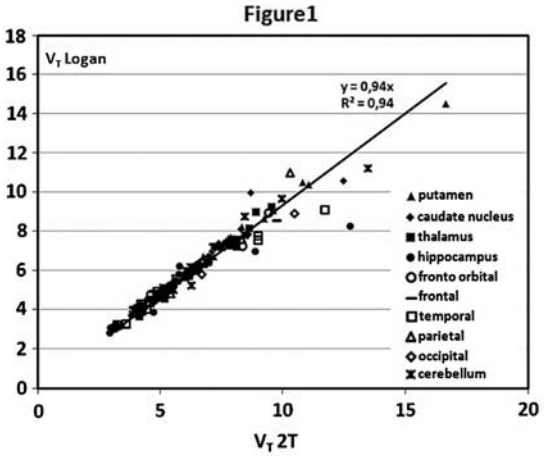

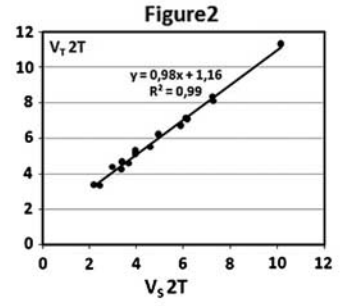

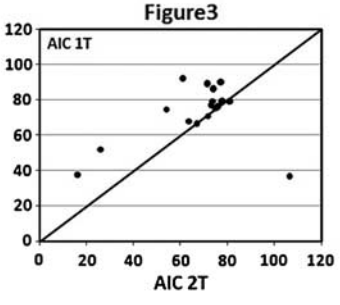

based on the Akaike Information Criterion (AIC) [2] in all but one dataset (see Figure 3).
Conclusions: Baseline dynamic brain PET in healthy volunteers indicate that the tracer kinetics of [^{11}C]JNJ42491293 in the human brain can be analyzed by a 2 tissue compartment model or by Logan plot, providing estimates of V_T.

References

[1] Watabe H, Channing MA, Der MG et al. Kinetic analysis of the 5-HT2A ligand [11C]MDL 100,907. J *Cereb Blood Flow Metab* 2000; 20(6):899–909.
[2] Akaike, H. A new look at the statistical model identification. IEEE Trans. *Automat Contr* 1974, AC19:716–723.

O20. PET imaging of the metabotropic glutamate receptor type 5 in cocaine abuse

Diana Martinez[1], Yiyun Huang[2], Mark Slifstein[1], Nina Urban[1], Alex Grassetti[1], Audrey Perez[1], Nabeel Nabulsi[2] and Richard Carson[2]

[1]Columbia University/NYSPI, New York, New York, USA; [2]Yale University PET Center, New Haven, Connecticut, USA

Background: Previous preclinical studies show that the mGluR5 plays a crucial role in addiction. In rodent and non-human primates, mGluR5 antagonist administration decreases cocaine seeking behavior. In addition, studies in rodents have shown that chronic cocaine exposure and withdrawal reduced mGluR5 receptor expression in the striatum. The goal of this study was to compare mGluR5 receptor binding in human chronic cocaine abusers with healthy control volunteers.
Methods: Fifteen currently active, chronic cocaine abuses and 13 healthy control subjects completed the study. The cocaine abusers were admitted to the inpatient unit at the New York State Psychiatric Institute for 10–13 days prior to the PET scans to ensure abstinence. Healthy control subjects were matched for age, gender, ethnicity and cigarette smoking and participated as outpatients. All subjects were scanned with [11C]ABP688, using a bolus with constant infusion, and an arterial input function was obtained. Each subject's MRI was obtained for delineation of the regions of interest, which included the striatal subdivisions and other cortical and subcortical regions. MGluR5 receptor availability was estimated using the binding potential relative to non-specific binding (BPND) in the regions of interest. The volume of distribution for the reference region (cerebellum) was obtained.
Results: The values for BPND were significantly lower for the cocaine abusers compared to the control subjects in each of the striatal regions of interest ($p < 0.001$ prior to correction for multiple observations). Measuring the striatum as a whole, the cocaine abusers had an average decrease of 22% compared to the control group ($p = 0.006$). In addition, the BPND for [11C]ABP688 was lower in most of the remaining regions of interest in the cocaine abusers compared to healthy controls.
Conclusions: In chronic cocaine abusers, mGluR5 receptor BPND, measured with [11C]ABP688, is reduced compared to matched control subjects. This finding is similar to previous studies in rodents, reporting reduced levels of mGluR5 in the striatum.

21. Examination of structural connectivity in depression: anti-depressant remitters versus non-remitters

Christine DeLorenzo[1], Jeffrey Miller[1], Matthew Milak[1,2], Binod Thapa-Chhetry[1], J. John Mann[1,2] and Ramin Parsey[1,2]

[1]Columbia University, New York, New York, USA; [2]New York State Psychiatric Institute, New York, New York, USA

Background: We have shown that patients with major depressive disorder who do not remit (non-remitters) to selective serotonin reuptake inhibitors (SSRIs) have lower $5HT_{1A}$ binding in regions such as the amygdala and hippocampus than those who do (remitters). This decrease in $5HT_{1A}$ binding may be due to either a diminished number of serotonergic fibers (originating from the raphe in the midbrain) or reduced $5HT_{1A}$ expression. These possibilities can be examined using Diffusion Tensor Imaging (DTI), which identifies fiber tracts between regions by measuring the diffusion of water molecules in the brain [1]. Fractional anisotropy (FA), a DTI-derived measure of the lack of free diffusion of water, can

then be used as an index of the health of the identified tracts [1].

Methods: Eighteen subjects with major depressive disorder received 25-direction DTI and Positron Emission Tomography (PET) scans prior to 65 ± 11 days of treatment with an SSRI. Severity of depression was assessed with the 24-item Hamilton Depression Rating Scale (HDRS) before and after treatment, with remission defined *a priori* as a 50% decrease in HDRS and a final score ≤ 10. Raphe nuclei were extracted from the [^{11}C]-WAY-100635 PET image [2] and included within a midbrain region of interest. Probabilistic tractography was performed between the midbrain (seed) and the amygdala or hippocampus (targets) (see Figure 1). Average FA values, which range from 0 to 1, were calculated by taking the mean of voxel FA values within the defined fiber tracts, weighted by the number of fibers crossing through that voxel.

Results: Average FA in fiber tracts to the right amygdala target was significantly lower in non-remitters (0.51 ± 0.05) versus remitters (0.58 ± 0.05, $p < 0.01$). At a trend level, both the number of tracts to the amygdala targets ($p = 0.13$, right, $p = 0.08$, left) and the average FA in tracts to the left amygdala target ($p = 0.16$) were also lower in non-remitters. No significant differences were found in average FA values, or number of tracts, to the right or left hippocampus target.

Conclusions: These results suggest that the health and/or number of serotonergic fibers terminating at the amygdala may be compromised in SSRI non-remitters. Moreover, since these differences were not observed in tracts terminating at the hippocampus, this effect may be regional. Future studies are needed to confirm this relationship in a larger cohort, examine these findings in healthy volunteers, and determine whether treatment affects this abnormality.

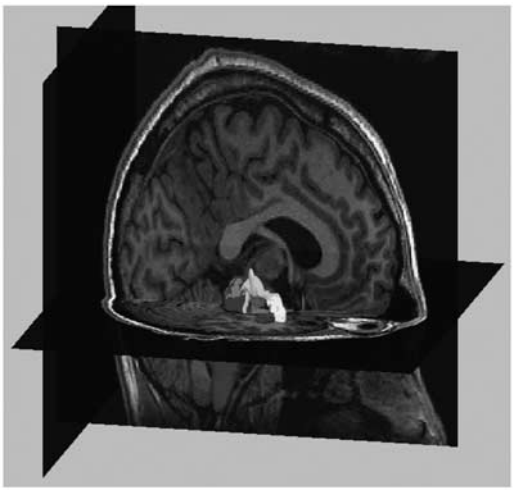

Figure 1 Example of tractography results in one subject. The magnetic resonance image (MRI) of one subject is shown. (Cutaway views of a sagittal and axial slice.) Overlaid on the MRI are volume renderings of the midbrain (white) containing the raphe nuclei (dark regions), the right amygdala (grey), and the tracts between these regions (black). At each voxel, the number of tracts between midbrain and right amygdala were determined and used as weighting factors in the calculation of average fractional anisotropy. Only voxels containing more than 40 tracts are shown.

References

1) Beaulieu C (2002) *NMR in Biomedicine* 15(7–8):435–55.
2) Mathis *et al.* (1994) *Life Sciences* 55(20):PL403–7.

O22. Treatment response in major depression predicted by serotonin transporter interplay

Rupert Lanzenberger[1], Georg S. Kranz[1], Daniela Haeusler[2], Elena Akimova[1], Markus Savli[1], Andreas Hahn[1], Markus Mitterhauser[2], Christoph Spindelegger[1], Wolfgang Wadsak[2] and Siegfried Kasper[1]

Medical University of Vienna, Austria: [1]Department of Psychiatry and Psychotherapy; [2]Department of Nuclear Medicine

Background: Recent mathematical models suggest that restored serotonergic bursts underlie the antidepressant effect of selective serotonin reuptake inhibitors (SSRI) [1,2]. Burst recovery is tuned to a down-regulation of serotonin transporter (SERT) availability in terminal regions and this may highly depend on the interregional balance between SERT availability in the raphe nuclei and in terminal regions before treatment. To evaluate this in humans, we investigated SERT availability and occupancy longitudinally in patients with major depressive disorder.

Methods: Using positron emission tomography (PET) and the radioligand [^{11}C]DASB, measurements were performed before and after a single oral dose, as well as after three weeks (mean 24.73 ± 3.3 days) of continuous oral treatment with either escitalopram (10 mg/day) or citalopram (20 mg/day). Data were analyzed using voxel-wise linear regression and ANOVA to compare SERT binding and binding ratios.

Results: Brain areas showing significant differences (ANOVA) between responders and non-responders

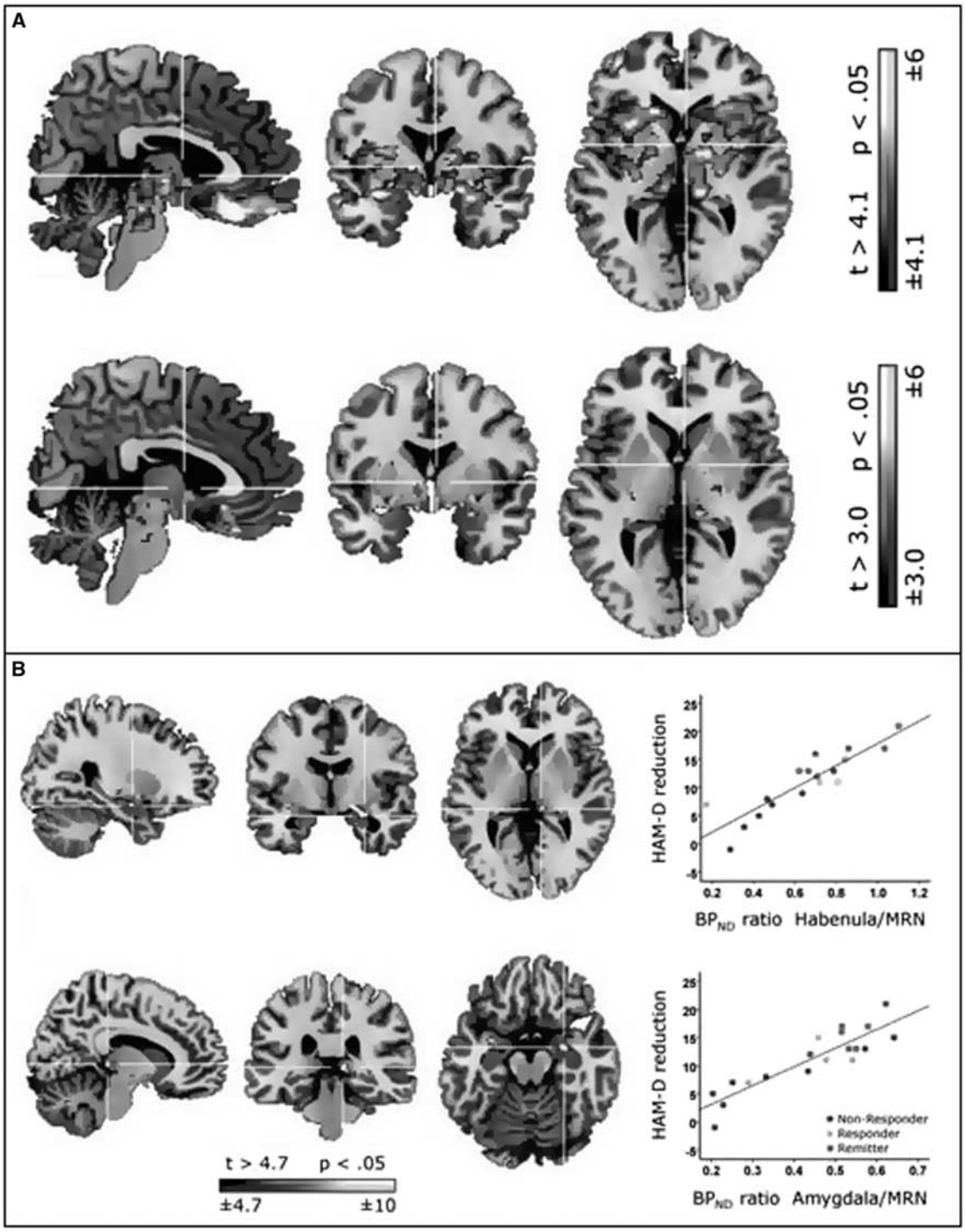

Figure A Brain areas showing significant differences between responders (n = 11) and non-responders (n = 8) (upper row) and between remitters (n = 7) and non-responders (bottom row) for SERT BP_{ND} ratios. T-values in the colour table ranging from ± 3.0 to ≥ ± 6). All p-values are FDR corrected ($p < 0.05$, cluster size ≥30 voxels, model corrected for age and escitalopram in plasma). Treatment responders had a 50% or greater reduction relative to initial HAM-D scores and remitters displayed a final HAM-D score of ≤7. The highest peaks were found in the sgACC and orbitofrontal cortex, habenulae, amygdalae, anterior insula, striatum and midbrain. **Figure B** Brain areas showing significant associations between pretreatment SERT binding ratios and treatment response, corrected for age and S-citalopram in plasma. T-values are given in the color table. (*Left*) Statistical parametric maps (SPM) showing highest associations in both amygdalae (upper row) and in both habenulae/epithalami (bottom row). (*Right*) Scatterplots depicting the relationship between absolute HAM-D reduction and pretreatment SERT binding ratios at the peak voxel (see crosshair). Significance corresponds to a FDR threshold $P < 0.05$, corrected for multiple comparisons.

and between remitters and non-responders for SERT BP_{ND} ratios (SERT BP_{ND} in the whole brain normalized to SERT BP_{ND} in the median raphe nucleus) are given in Figure A. Regression analyses revealed that lowered SERT availability in the median raphe compared to SERT availability in key regions for depression such as the habenula, amygdala–hippocampus complex, and subgenual cingulate cortex highly predicted the antidepressant response (see Figure B).
Conclusions: Our data provide a first proof-of-concept for recent modeling studies and further underlie the importance of the habenula and subgenual cingulate cortex in the etiology of and recovery from major depression [3]. These findings may indicate a promising molecular predictor of treatment response and stimulate new treatment approaches based on regional differences in SERT binding.

References

[1] Best J et al. *Pharmacopsychiatry* 2011; 44(Suppl 1): S76-83.
[2] Best J, Nijhout HF, Reed M. *Theor Biol Med Model* 2010; 7:34.
[3] Mayberg HS. *J Clin Invest* 2009; 119(4):717-25.

O23. PET imaging of serotonin transporter in monkeys: effects of maternal separation, and long-term fluoxetine treatment during adolescence

Saurav Shrestha, Jeih-San Liow, Robert Gladding, Victor Pike, Pam Noble, James Winslow, Eric Nelson, Steve Suomi, Daniel Pine and Robert Innis

National Institutes of Health, Bethesda, Maryland, USA

Background: Major depressive disorder (MDD) is a serious disorder that often begins following stress during adolescence. Selective serotonin reuptake inhibitors (SSRIs) are a common treatment for both adolescent and adult MDD. While MDD's early onset and available efficacy data support use of SSRIs in adolescents, concerns about safety have arisen, based on associations with suicidal behavior in adolescents, coupled with minimal data on long-term effects on the developing brain. This study used rhesus monkeys as a model to study the long term effects of both early life stress and chronic antidepressant treatment during adolescence (2-year of age) on the serotonin transporter.
Methods: Thirty-two monkeys were randomly assigned to one of four groups (8 monkeys/group). They were peer-reared (PR) vs. mother-reared (MR), and with or without fluoxetine treatment. For PR, monkeys were separated from mothers at birth and nursery-reared until 6 months of age and thereafter housed with their peers. Chronic fluoxetine treatment began at 2-year of age for one year. One to two years post-washout, monkeys (average age of 5) were scanned with Positron Emission Tomography (PET) using [11C]DASB for serotonin transporter (SERT).
Results: Our data from 32 monkeys (8 in each group) show 1. A significant global decrease in SERT binding in PR compared to MR monkeys, and 2. SERT binding is reversed in PR monkeys that received fluoxetine treatment.
Conclusions: Our study demonstrates serotoninergic alterations in PR monkeys, and chronic fluoxetine treatment may reverse deficits in SERT density that is persistent more than one year after medication discontinuation.

O24. Serotonin-1A receptor-dependent modulation of the default mode network

Andreas Hahn[1], Wolfgang Wadsak[2], Christian Windischberger[3], Pia Baldinger[1], Lukas Nics[2],Georg Kranz[1], Johanna Ungersboeck[2], Markus Mitterhauser[2], Siegfried Kasper[1] and Rupert Lanzenberger[1]

Medical University of Vienna, Austria: [1]Department of Psychiatry and Psychotherapy; [2]Department of Nuclear Medicine; [3]MR Center of Excellence, Center for Medical Physics and Biomedical Engineering

Background: Despite the growing interest in functional connectivity networks the underlying neurochemical mechanisms largely remain unknown. These networks are commonly assessed by spontaneous fluctuations in BOLD signal, which is in turn regulated by glutamate signaling and monoamine neurotransmitters as serotonin [1]. Hence, we evaluated local and autoinhibitory effects of the serotonin-1A receptor (5-HT1A) on the default mode network (DMN).
Methods: Twenty-eight healthy subjects (mean age ± SD = 26.5 ± 6.8 years, 11 male) underwent fMRI and

PET with the radioligand [carbonyl-11C]WAY-100635. 5-HT1A binding potentials (BPND) were quantified using the Logan non-invasive model with cerebellar gray matter (excl. vermis) as reference in PMOD3.3. 5-HT1A autoreceptor binding was estimated with a 4 mm spherical region-of-interest placed manually in the dorsal raphe nucleus. Voxel-wise BPND maps were computed to assess local 5-HT1A heteroreceptor binding in projection areas. The DMN was calculated by functional connectivity analysis from a 6 min resting-state fMRI scan in Matlab/SPM8. Preprocessing included regression against white matter, ventricular and global signal, movement parameters and bandpass filtering ($0.007 < f < 0.08$ Hz). To avoid seed selection bias, the BOLD signal was averaged across the entire network (intersection of group maps from seeds in posterior cingulate (PCC) and medial prefrontal cortices (mPFC), $p < 0.05$ FWE-corrected) followed by whole-brain cross-correlation and z-transformation. Associations between serotonin-1A bindings and the DMN were assessed by voxel-wise linear regression analysis with the biological parametric mapping toolbox. Entering both 5-HT1A dorsal raphe autoreceptor and local heteroreceptor binding into the model enables an evaluation of the two variables as independent predictors of DMN activity (i.e., adjusting for regional heteroreceptor binding when interpreting 5-HT1A autoinhibition and vice versa).

Results: For local 5-HT1A heteroreceptors we found a positive modulation of the DMN in the retrosplenial cortex (RSC, $r = 0.8$, $p < 0.05$ FWE-corrected) and a negative association in the dorsal mPFC ($r = -0.67$, $p < 0.001$ uncorrected). In contrast, both 5-HT1A auto- and heteroreceptor binding predicted individual DMN activity in the PCC but in an inverse manner ($r = 0.74$, $p < 0.05$ FWE-corrected and $r = -0.66$, $p < 0.001$ uncorrected, respectively; see Figure).

Conclusions: This work demonstrates a distinctive 5-HT1A regulation of various DMN regions, which are involved in episodic memory processing (RSC), self-referential judgements (dmPFC) and the evaluation of personal significance of events (PCC). Moreover, the inverse DMN modulation of dorsal raphe autoreceptors and local heteroreceptors in the PCC (the strongest hub in the human brain) suggests a well-balanced interaction between local and autoinhibitory 5-HT1A effects. 5-HT1A autoreceptors attenuate raphe cell firing, leading to reduced serotonin release at projection sites [2]. This decreases local 5-HT1A inhibition onto downstream glutamate neurons, which in turn increases the BOLD signal [1]. Together with previous findings this study indicates a modulation of brain networks by complex distribution of neuronal receptors including expression sites on downstream glutamate and GABA neurons [3].

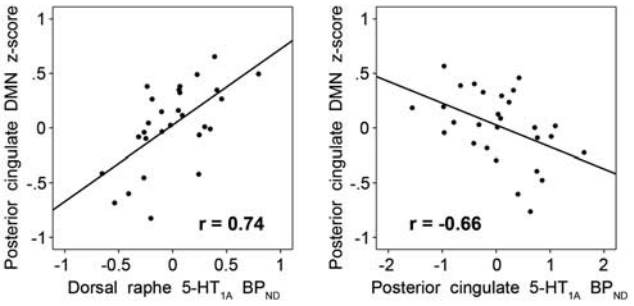

Figure Partial regression plots show associations between 5-HT1A BPND and the default mode network. The posterior cingulate cortex is modulated via both dorsal raphe nucleus autoreceptors (left, $r = 0.74$) and local heteroreceptors (right, $r = -0.66$), suggesting a well-balanced interaction between local and autoinhibitory 5-HT1A effects. Note that values are mean-centered after correction for nuisance variables.

References

[1] *Trends Neurosci* 25(12):621–625, 2002.
[2] *Eur J Pharmacol* 590(1-3):136–149, 2008.
[3] *Nat Neurosci* 10(12):1515–1517, 2007.

O25. Estimation of the linearity point in graphical analysis

R. Todd Ogden[1] and Yuichi Kimura[2]

[1]Columbia University/NYSPI, New York, New York, USA; [2]National Institute of Radiological Sciences, Chiba, Japan

Background: A popular alternative approach to full kinetic modeling is the so-called ''graphical approach'' [1] which is based on the approximate linear relationship between transformations of the plasma and brain concentration functions and for which the volume of distribution VT is equal to the slope of the relationship. This approximation improves as time t increases, and thus it is necessary to choose some cutoff time point t*, i.e., the graphical approach will consider only those points for which $t > t^*$. If t* is chosen to be too small, the approximation is poor and therefore the estimate of VT will be biased. Conversely, if t* is chosen to be too large, the variance of VT will be higher because too few points are used in fitting. In such a graphical approach, it is common to select the value of t* based on visual inspection of a plot the transformed data. While this may be appropriate in low-noise situations, it is subjective and would not be practical when fitting many time-activity curves. Though some automatic procedures for

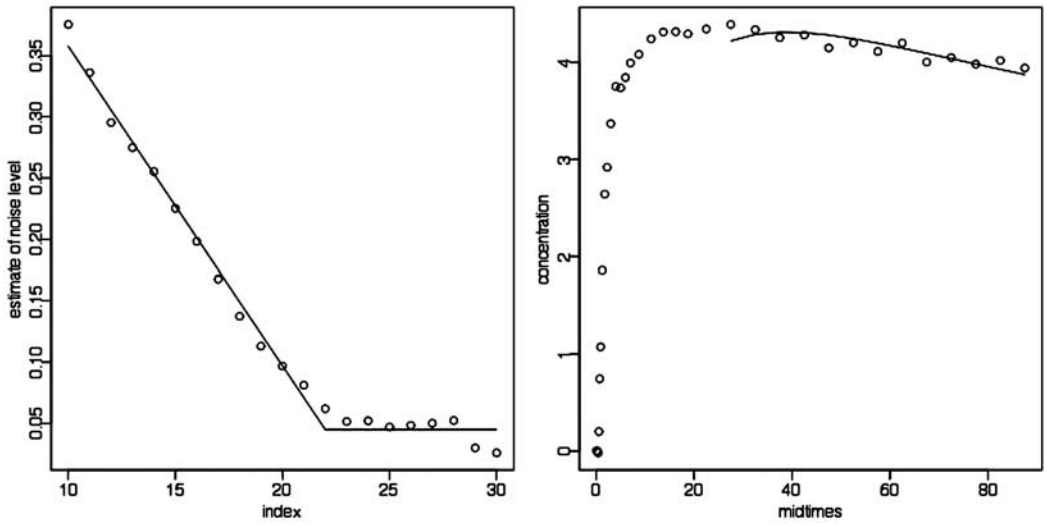

Figure (Left panel) Estimates of the noise level for each timepoint index with the fitted onset-of-trend change-point model superimposed. (Right panel) Corresponding fit of the time-activity curve based on a graphical model with the estimated t* value.

choosing t* are in use (as in PMOD), some specification of an arbitrary threshold (e.g., a bound on the limit of the relative size of residuals) is required.
Methods: We propose an alternative completely automatic approach that is based on how well the graphical model fits the data. For each candidate t* value, we fit the data points corresponding to $t > t^*$ according to a likelihood-based procedure for graphical analysis [2] and calculate an estimate of the noise level. When considering candidate cutoff times greater than the true t*, these variance estimates will have a common mean, but for a candidate cutoff less than the true t*, these estimates will be biased upwards, with the bias increasing as the candidate t* value decreases.
Results: An automatic procedure for choosing the optimal t* based on this sequence of noise level estimates results from casting the problem as a problem in change-point estimation. In particular, we will estimate t* by applying an onset-of-trend change-point model [3] to the estimates of the noise level.
Conclusions: We explore the properties of this procedure with a simulation study (for which the ''truth'' is known) and demonstrate its performance on data from a PET human study of the sigma-1 receptor using [11C]SA4503 [4].

References

[1] Logan et al. (1990). *JCBFM* 10:740–747.
[2] Ogden (2003). *Statistics in Medicine* 22:3557–3568.
[3] West and Kodell (2005). *JABES* 10:197–211.
[4] Sakata et al. (2007). *Neuroimage* 35:1–8.

O26. Limitations of SRTM, Logan plot, and equilibrium analysis for measuring transient dopamine release in [^{11}C]raclopride PET studies

Jenna M. Sullivan[1], Su Jin Kim[1], Kelly P. Cosgrove[1,2] and Evan D. Morris[1,2]

[1]Yale PET Center, Yale University, New Haven, Connecticut, USA; [2]Department of Psychiatry, Yale University, New Haven, Connecticut, USA

Background: Conventional PET methods to estimate [^{11}C]raclopride BP_{ND} assume that endogenous dopamine (DA) concentration does not change during the scan time. However, this assumption is purposely violated in studies which use pharmacological or behavioral stimuli to invoke DA release. When the assumption of steady-state DA is violated, conventional analysis methods may produce biased and even unusable estimates of BP_{ND}. To illustrate this problem, we examined the effect of scan duration on ΔBP_{ND} estimated by three common analysis methods (SRTM, Logan with reference region, and equilibrium analysis) applied to (simulated and real) single-scan activation studies.
Methods: Noiseless striatal [^{11}C]raclopride time activity curves (TACs) were simulated with an enhanced tracer kinetic model including time-varying DA. Bolus plus constant infusion (B/I) TACs were simulated over 120 min. DA was modeled as a gamma variate with release commencing at 40 min. Because nicotine has been shown to cause transient DA release in the striatum (Sziráki, 1998) our

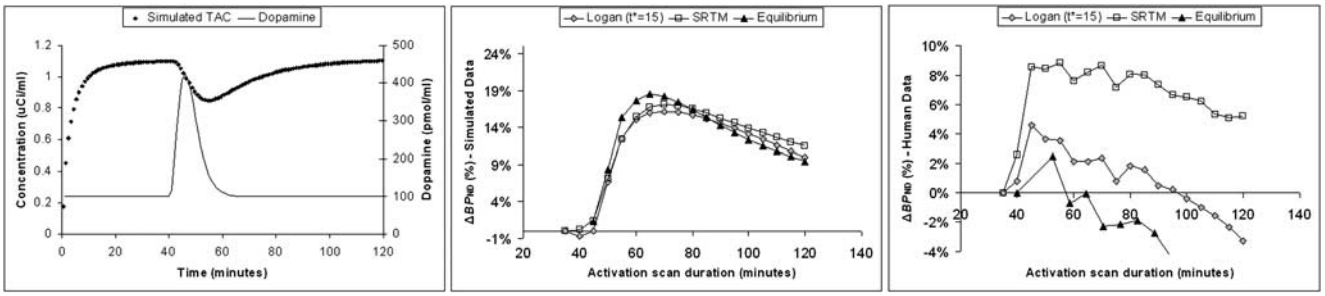

Figure (Left) Simulated, noiseless, striatal TAC and DA curve. (Middle) Effect of scan duration on ΔBP_{ND}. ΔBP_{ND} was calculated as 1-($BP_{ND}^{Activation}/BP_{ND}^{Baseline}$). For better pattern visualization, equilibrium results are placed on the same x-axis as Logan and SRTM. (Right) A similar pattern is seen in Logan and SRTM analysis of human smoking data from the left ventral striatum. This pattern of ΔBP_{ND} change is less apparent in the equilibrium approach but a time-dependence is still evident.

simulated DA curves were short (~20 min FWTM). TACs were simulated for multiple DA release patterns. For SRTM and Logan reference (t* = 15), ΔBP_{ND} was calculated as the percent difference between baseline BP_{ND} (using 0–35 min of the TAC) and activation BP_{ND} estimated from varying scan durations greater than 40 min. For the equilibrium approach, baseline BP_{ND} was an average over 30–40 min and activation BP_{ND} was an average from 45 min to the end of the data. Data from a healthy human subject who received a B/I of [^{11}C]raclopride (20mCi) were analyzed similarly. The subject smoked 2 consecutive cigarettes in the HRRT, beginning 45 min after [^{11}C]raclopride. Head motion was recorded using an optical tracking system and rigid tool attached to the subject's head. Dynamic data were reconstructed iteratively with MOLAR, including all standard corrections.

Results: Simulations showed ΔBP_{ND} to be highly dependent on duration of data used to determine BP_{ND} in the activation state. This was true for all DA signals tested. The pattern of ΔBP_{ND} mirrored the shape of the DA signal. ΔBP_{ND} tended to peak 10 min after DA take-off. A similar pattern was seen in the human data. No such pattern of ΔBP_{ND} dependence on duration of data was apparent in simulations where DA was held constant.

Conclusions: The dependence of ΔBP_{ND}, as estimated by SRTM, Logan, and equilibrium methods, on the duration of data analyzed illustrates the inability of these conventional methods to reliably quantify short-lived increases in endogenous DA. More complicated models which take into account time-variation in DA are needed to properly measure the effect of stimulus-induced DA release when the DA response is brief.

O27. Validation of the partial saturation approach for *in vivo* quantification of striatal dopamine D2 receptors with [^{11}C]raclopride

Catriona Wimberley[1], Kristina Fischer[2], Bernd J. Pilcher[2] and Marie Claude Gregoire[3]

[1]Brain and Mind Research Institute and Faculty of Health Sciences, University of Sydney, Australia; [2]Department of Preclinical Imaging and Radiopharmacy, Laboratory for Preclinical Imaging and Imaging Technology of the Werner Siemens-Foundation, Eberhard-Karls University of Tuebingen, Germany; [3]Life Sciences Division, Australian Nuclear Science and Technology Organisation, Australia

Background: [^{11}C]Raclopride is a commonly used radiotracer for the *in vivo* quantification of Dopamine D2 receptor binding. The partial saturation approach (PSA) has been proposed to assess the appBmax and appKd in a single injection protocol [1]. Previously this method was successfully adapted for a range of receptor occupancy levels in healthy animals [2]. Fischer et al. [3] conducted a series of experiments measuring pharmacologically induced changes of synaptic DA concentrations in wild type and two transgenic mouse models. The aim of this study was to confirm that the PSA also produces stable and accurate parameter estimates in pharmacological or disease-induced changes in appBmax and appKd for [^{11}C]raclopride in the rodent.

Method: The PSA uses the general equilibrium equation (B/F = (Bmax-B)/KdVr – dB/dT * (1/koff*F)) which includes a residual term as an indicator of the dynamic equilibrium state. For the dynamic equilibrium assumption to be met, the residual term should be within a certain small value [2]. Simulations: A series of partial saturation experiments with noise level equivalent to that of the PET (100 noise simulations per experiment) were simulated over a

range of receptor occupancies for three appBmax levels and three appKd levels (normal, double and half) to mimic the expected levels in the experiments by Fischer et al. [3]: (i) 12 mice underwent one scan at baseline and one under challenge conditions (AMPH or Methylphenidate) (ii) two mouse models (n = 15) of human disease (Parkinson's and Huntington's disease). The parameters appBmax and $appK_d$ were estimated for each simulated experiment using the equilibrium relation for (i) a time window driven by constraining the residual term and (ii) a static time window of 10–50 mins.

Results: Simulations: Figure 1 shows the difference between the appBmax estimates and the true Bmax for 4 of the simulations, high and low appBmax and appKd and for all occupancies with a fixed and guided time window. The improvement in accuracy when using the guided window seen in the appBmax estimates is echoed in the appKd estimate (not shown) and the improvement in accuracy can be seen in all appBmax/appKd levels simulated (not shown) with mean values that sit within 5-10% of the true appBmax/appKd values at occupancy levels >50% and within 15% at occupancy levels of 30&40%. Experimental data: Please refer to the abstract by Fischer et al. for the results of the experimental data [3].

Conclusions: Our results demonstrate that the PSA with a guided time window produces accurate and stable estimates where large variations of appBmax and appKd are expected. The method is promising for assessing changes in appBmax and appKd after pharmacological interventions and in models of neurodegenerative disorders.

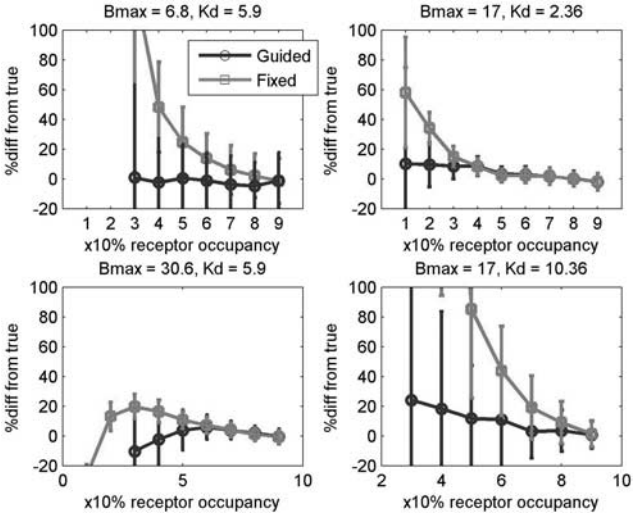

Figure 1 appBmax estimates.

References

[1] Delforge et al. *J Nucl Med* 1996; 37:5–11.
[2] Wimberley et al. World Molecular Imaging Congress 2011, San Diego.
[3] Fischer et al. *J Cereb Blood Flow Metab* 2012, Suppl, NRM2012.

O28. Update: inhibition plots of [^{11}C]yohimbine binding yield consistent estimates of non-displaceable volumes of distribution in multiple tests

Anne M. Landau[1], Suzan Dyve[1,2], Steen Jakobsen[2], Aage Ko Alstrup[2], Doris Doudet[3] and Albert Gjedde[1,4,5,6]

[1]Aarhus University, Denmark; [2]Aarhus University Hospitals, Denmark; [3]University of British Columbia, Vancouver, Canada; [4]University of Copenhagen, Denmark; [5]McGill University, Montreal, Canada; [6]Johns Hopkins University, Baltimore, Maryland, USA

Background: The inhibition plot version of the Lassen family of plots (Cunningham et al. 2011) is useful when the non-displaceable volume of distribution (V_{ND}) of a tracer in brain is unknown. The original form of the inhibition plot differs from other forms by not commingling the independent and dependent volumes of distributions (Gjedde & Wong 2000), in the absence and presence of displacement, $V_{T(baseline)}$ and $V_{T(inhibition)}$. The inhibition plot linearizes to the form, $V_{T(inhibition)} = (1\text{-}s)\ V_{T(baseline)} + s\ V_{ND}$ where s is the saturation of the receptor in question. Linear regression to matching measures of $V_{T(baseline)}$ and $V_{T(inhibition)}$ yields independent estimates of s and V_{ND} which serve to calculate binding potentials (BP_{ND}). We applied this inhibition plot to the novel PET tracer [^{11}C]yohimbine as a selective antagonist of the alpha-2 adrenoceptors in pigs. In this test, we used vagal nerve stimulation (VNS) to elevate noradrenaline in cerebral cortex.

Methods: Four groups of pigs underwent inhibition by exogenous competition with data from Landrace pigs published by Jakobsen et al. (2006), inhibition after amphetamine with two groups of data, including data from Landrace pigs published by Landau et al. (2012) and unpublished observations in minipigs, and inhibition by VNS based on unpublished observations in minipigs with stimulators implanted in the chest wall. Briefly, the pigs were premedicated and anesthetized and fitted with a vagal nerve stimulator (Cyberonics, Inc) in the back of the

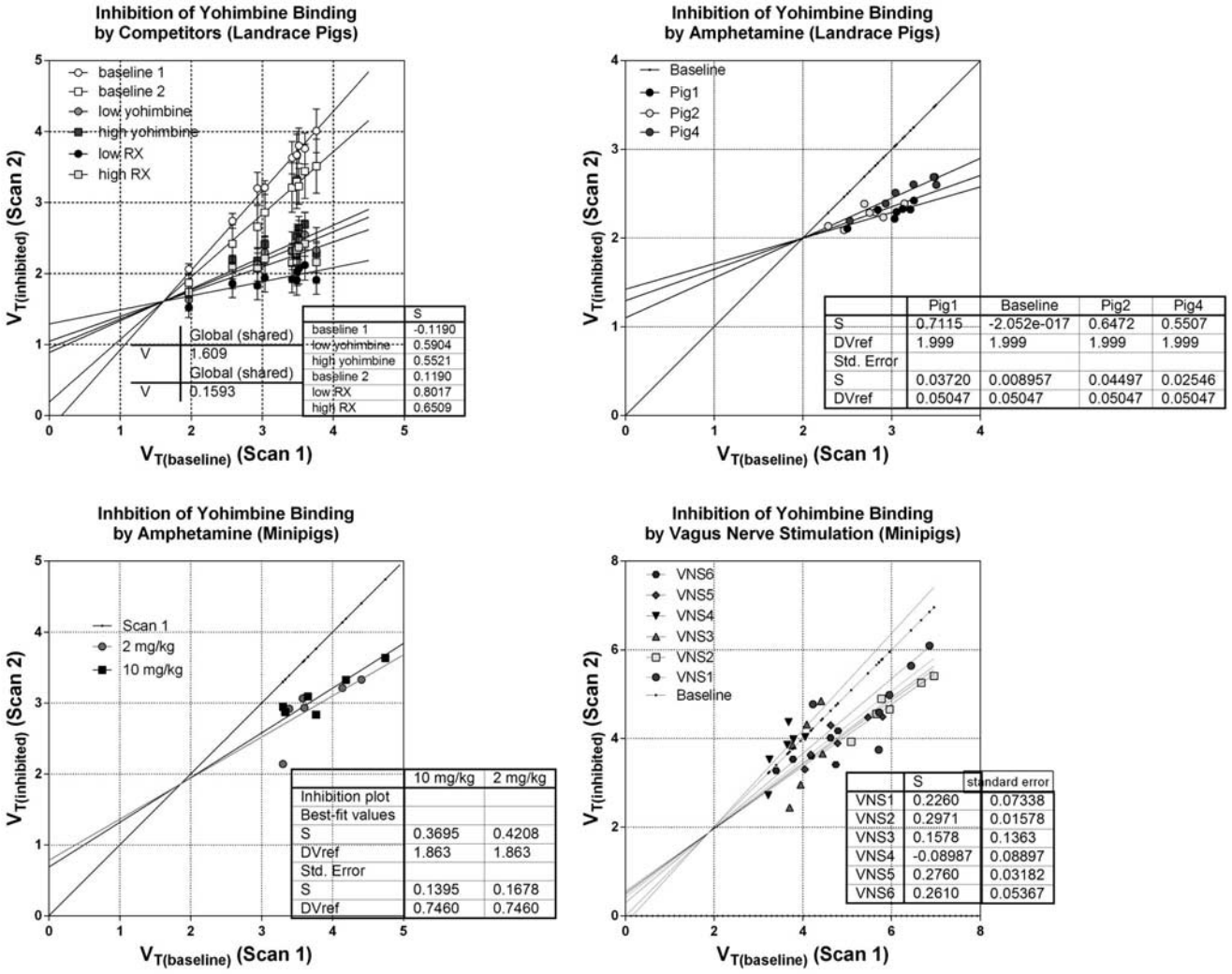

Figure The four panels of the figure (clockwise from upper left panel) display, respectively, 1) inhibition by exogenous competitors in Landrace pigs, 2) inhibition by amphetamine in Landrace pigs, 3) inhibition by VNS in minipigs, and 4) inhibition by amphetamine in minipigs.

neck. After 4-6 weeks of recovery in the baseline OFF condition and 30 minutes in the acute ON condition with 1.0 mA stimulation, dynamic PET began at injection of high specific activity (>50 GBq/μmol) [^{11}C]yohimbine with multiple frames increasing in length until 90 min. In the tests of amphetamine, animals received standard doses of 2 or 10 mg/kg d-amphetamine i.v. 20 minutes before the second [^{11}C]yohimbine PET. We obtained the total volume of distribution (V_T) for each region with the Logan graphical analysis during the 25–90-min post-[^{11}C]yohimbine injection period with an arterial input function.

Results: As illustrated in the four panels of the Figure (groups 1-4, clockwise from upper left panel), exogenous competitors occupied from 55% to 80% of the alpha-2 adrenoceptors with a V_{ND} estimate of 1.6 ml/g. In the first amphetamine challenge with 10 mg/kg amphetamine, the putative endogenous ligand(s) occupied from 55% to 70% of the receptors, and in the second challenge with 2 and 10 mg/kg, from 35% to 40%. The non-displaceable volumes averaged 1.9 to 2.0 ml/g. With the average value of 1.8 ml/g, the acute vagal nerve stimulation led to an average saturation of 19% of the receptors.

Conclusions: The inhibition plot is the simplest approach to the determination of binding potentials and saturability of neuroreceptors, when reference regions are not available, i.e., areas of the brain with no displaceable binding of the ligand. With volumes of distribution of 2-4 ml/g in Landrace pigs, and 3-6 ml/g in minipigs, corresponding binding potentials range from 0.1 to 1 in landrace pigs and 0.5 to 2 in minipigs.

O29. The detectability of Aβ amyloid by Florbetapir F18 PET imaging in mouse models of Alzheimer's disease with different rates of plaque accumulation

Alena Savonenko, Ayon Nandi, Heather Valentine, Tatiana Melnikova, Eugenia Cho, Deidre Lee, Don Price and Dean F. Wong

Johns Hopkins University School of Medicine, Baltimore, Maryland, USA

Background: Formation of senile plaques composed of Aβ peptides, a pathological hallmark of Alzheimer's disease (AD), precedes the onset of symptoms by years. Development and validation of non-invasive detection methods for Aβ plaques in the human brain would allow for a presymptomatic diagnosis and early preventive treatments. In addition to clinical applications, the successful establishment of *in vivo* Aβ plaques detection in brains of mouse models of AD will be a powerful step in the development of new therapeutic treatments and markers of its efficacy. Importantly, using the same tracers in human and mouse studies would allow for the correlation of imaging data with the morphological and immunohistochemical data from animal studies. One of the most successful noninvasive techniques so far to visualize Aβ plaques in patients with AD is PET imaging with C^{11}-PIB tracer. However, in addition to C^{11}-PIB's short half-life, the limitations of this tracer include a low sensitivity to Aβ plaques in brains of AD mouse models. In this study, we tested a reliability of microPET in mice using F^{18}-Florbetapir tracer. We hypothesize that by virtue of its longer half-life, F^{18}-Florbetapir tracer can provide more favorable conditions to meet the requirement of high specific activity to Aβ that is difficult to achieve with C^{11}-PIB tracer. In the case of ^{11}C-PIB tracer, Maeda and colleagues (2007) had suggested that this tracer is particularly sensitive to such specific Aβ subtypes as N-terminally truncated and modified Aβ, AβN3-pyroglutamate. This type of amino-terminal modifications is a major component of human plaques (Saido et al., 1995) and is likely related to proteolytic activities of a number of proteases taking place over prolonged time (Iwata et al., 2005). In AD patients, the percentage of truncated and modified amino-terminus has been shown to increase at the expense of full length Aβ and is directly correlated with AD progression (Güntert et al., 2006). In APP transgenic mice, the occurrence of N-terminally truncated Aβ species was demonstrated to be decreased in comparison with human AD cases (Kuo et al., 2001; Rüfenacht et al., 2005). These findings imply that the detectability of Aβ amyloid by ^{11}C-PIB PET can differ in Alzheimer's disease (AD) and Tg mouse brains due to differential presence of modified Aβ species (Kuo et al., 2001; Kawarabayshi et al., 2001; Güntert et al., 2006).
Methods: Thus, in this study, we tested a hypothesis that mouse models of AD with fast rate of amyloid plaque deposition yield lower F^{18}-Florbetapir PET signal than models with slow accumulation. To this end, we compared two AD models, TetOffAPP Line 107 and PrP APPPS1 Line 85, with high and low rates, respectively.
Results: PrP APPPS1 Line 85 mice had a significantly higher signal in cortex, hippocampus and other forebrain structures supporting our hypothesis.
Conclusions: These studies validate the use of F^{18}-Florbetapir for the visualization of mouse amyloid by PET imaging and open a new avenue for a wide use of this tracer in monitoring the dynamics of amyloid deposition in living brains of AD mice.

References

Maeda et al. 2007, *J Neurosci* 27:10957-10968.
Saido et al. 1995, *Neuron* 14:457-466.
Iwata, et al. 2005, *Pharmacol Ther* 108:129-148.
Güntert et al. 2006, *Neuroscience* 143:461-475.
Kuo et al. 2001, *Mol Med* 7: 609-618.
Rüfenacht et al. 2005, *J Mass Spectrom* 40:193-201.
Kawarabayshi et al. 2001, *J Neurosci* 21:372-381.

O30. [^{11}C]PiB PET and post-mortem measures of amyloid load: regional correspondence

Julie C. Price[1], William E. Klunk[2], Chester A. Mathis[1], Eric E. Abrahamson[3], Lisa A. Weissfeld[4], Oscar L. Lopez[3], Manik L. Debnath[2], Shao Li[2], Ronald L. Hamilton[5] and Milos D. Ikonomovic[3]

University of Pittsburgh, Pennsylvania, USA, Departments of: [1]Radiology; [2]Psychiatry; [3]Neurology; [4]Biostatistics; [5]Neuropathology

Background: An ongoing objective for amyloid imaging research is to better understand the relationship between *in vivo* imaging measures of fibrillar amyloid-beta (Aβ) deposition and postmortem assessments of amyloid load. This work relates [^{11}C]PiB PET retention measures to postmortem correlates of

amyloid load on a region-by-region basis for individuals who exhibited a range of amyloid load levels.
Methods: Dynamic [^{11}C]PiB (or PiB) PET imaging was performed for 6 subjects (S) over 90 min (n = 5) or 60 min (n = 1). Scanning occurred within a 42 month (mos) interval (INT) before death for patients with Alzheimer's disease (AD) and dementia with Lewy bodies (DLB): 1) AD (63 yrs, INT = 10 mos); 2) AD (58 yrs; INT = 42 mos); 3) DLB (77 yrs, INT = 18 mos); 4) AD (54 yrs, INT = 30 mos); 5) AD (74 yrs, INT = 11 mos); 6) AD (80 yrs, INT = 37 mos). PiB retention was measured using the reference Logan DVR (DVR60, n = 6), standardized uptake value ratio (SUVR60: 40-60 min, n = 6), and 90 min simplified reference tissue model DVR (SRTM2 DVR, n = 5), with cerebellum as reference region. Post-mortem Aβ plaque load was assessed by applying Aβ immunohistochemistry (4G8) and a highly fluorescent derivative of PiB (6-CN-PiB) to 12 μm paraffin sections of multiple cortical and subcortical regions-of-interest (ROIs). A ROI-labeled autopsy image guided ROI generation on the ante-mortem MR and sampling of the co-registered PET data. ROIs included key cortical gray matter rich areas (e.g., frontal cortex, FRC) and a white matter rich area (internal capsule). PiB data were corrected for atrophy-related CSF dilution. Although limited by sample size, relationships were examined using Pearson correlation.
Results: The frontal PiB DVR60 values were: 2.7 (S1), 2.0 (S2), 1.1 (S3), 1.4 (S4), 2.2 (S5), and 1.8 (S6). Relative consistency was observed for the 6-CN-PiB and 4G8 measures for each subject with higher loads for S1, S2 and S5 than for S3, S4, and S6; and this was consistent across all types of retention outcomes. Stronger relationships were observed between PiB and 6-CN-PiB than for 4G8. For the FRC, DVR60 comparisons yielded: $y = 0.12x + 1.22$, $R = 0.96$ (6-CN-PiB) and $y = 0.08x + 1.42$, $R = 0.67$ (4G8), while SUVR60 comparisons yielded: $y = 0.17x + 1.47$, $R = 0.95$ (6-CN-PiB) and $y = 0.13x + 1.65$, $R = 0.76$ (4G8). The absence of Aβ plaques and 6-CN-PiB labeling in postmortem tissues corresponded to PiB DVR60 values between 1.0-1.2. In white matter rich areas, the null-signal for postmortem outcomes coincided with PiB DVR values from 1.3-1.6 (Logan and SRTM2).
Conclusions: Good correspondence was generally observed between cortical PiB retention and both Aβ and 6-CN-PiB positive plaque loads. Closer association of PiB retention with 6-CN-PiB compared to 4G8-immunoreactive plaque load likely reflects the presence of diffuse (less fibrillar) Aβ immunoreactive plaques which are labeled weakly with 6-CN-PiB. Definition of *in vivo* amyloid detection thresholds requires evaluation of a larger and more variable sample and better understanding of the limits of *in vivo* detection achievable for a given PiB retention outcome.
Acknowledgements: Support provided by NIH (R01AG033042, P50AG005133, P01AG025204), Dana Foundation, Alzheimer's Association, GE Healthcare.

O31. Quantitative assessment of longitudinal amyloid imaging using [^{11}C]PIB: impact of flow variations

Ronald Boellaard, Rik Ossenkoppele, Nelleke Tolboom, Maqsood Yaqub, Philip Scheltens, Adriaan Lammertsma and Bart van Berckel

VU University Medical Center, Amsterdam, The Netherlands

Background: Several methods can be used for quantitative assessment of ^{11}C-Pittsburgh compound-B ([^{11}C]PIB) binding. Recently, it was shown that use of suboptimal methodology may result in false positive findings, increased variability across subjects and bias in observed longitudinal changes [Berckel et al. SNM2011]. The objective of this study was to assess the impact of flow variations on the measurement of longitudinal changes in specific [^{11}C]PIB binding derived from reference tissue based methods.
Methods: Two simulations were performed, one assuming different changes in flow in target (global cortical region) and reference regions (i.e. a change in R_1) at follow-up and another assuming the same change in flow in both regions (global flow change). Furthermore, it was assumed that BP_{ND} did not change at follow-up. Simulations were based on typical [^{11}C]PIB plasma input curves, microparameters and blood volume fractions obtained from dynamic 90 min PET studies of Alzheimer's disease (AD) patients. For both simulations SUV ratios (SUVr) were calculated for several uptake times (ranging from 30 to 90 min p.i.). For comparison, $BP_{ND} + 1$ was obtained using a basis function implementation of SRTM (RPM) based on the simulated 90 min reference and cortical time-activity curves. For both SUVr and $BP_{ND} + 1$, percent bias compared with 'true' (simulated) BPnd + 1 values was calculated. In addition, artificial percent change in SUVr or BPnd + 1 as a result of global or heterogeneous flow change are evaluated.
Results: Simulations revealed that SUVr values were highly dependent on uptake period, with biases of up to + 25%. Moreover, longitudinal changes in both K_1 (global flow changes) or R1 (differential flow changes) induced both positive and negative artificial changes in [^{11}C]PIB binding estimates based on SUVr of up to 10%. Biases in $BP_{ND} + 1$ were much smaller (< 5%) in all cases. These differences in flow

induced changes in SUVr and $BP_{ND}+1$ were in line with differences in SUVr and $BP_{ND}+1$ changes seen in longitudinal studies in AD patients, suggesting that flow effects may play a role in the latter studies. **Conclusions:** Choosing the right method for quantitative assessment of longitudinal changes in [^{11}C]PIB binding is of the utmost importance in the case of global or regional flow changes over time or as a result of treatment. For monitoring effects of novel anti-amyloid drugs, specific binding of [^{11}C]PIB should be determined using full kinetic analysis in combination with dynamic PET scans.

O32. Combined CBF and binding analyses with single ^{11}C-PIB PET session in Alzheimer's disease and healthy controls

Anders B. Rodell[1], Joel F. Aanerud[1], Hans Braendgaard[2] and Albert Gjedde[1,3]

[1]Dept. of Nuclear Medicine and PET Centre, Aarhus University Hospital, Denmark; [2]Dept. of Clinical Medicine, Dept. of Neurology, Aarhus University Hospital, Denmark; [3]BRAINlab, Dept. of Neuroscience and Pharmacology, University of Copenhagen, Copenhagen, Denmark

Background: The ^{11}C-labeled Pittsburg Compound B (PIB) is a tracer of A-beta plaque load used to diagnose Alzheimer's disease (AD). However, the rapid initial clearance of the tracer from the blood stream mimics the kinetic behavior of a microsphere with a very rapid distribution to the tissue, followed by washout that is almost solely governed by the flow-mediated clearance from the tissue. Previous studies used either Logan linearization (LL) for parametric mapping of the distribution volume (DV), or simple computation of a ratio measure (RM) of steady-state accumulation relative to a reference region such as the pons or cerebellum gray matter, using area-under-curve (AUC) values of late time (60-90 minutes). These methods are known to be clearly influenced by flow, and existing studies suggest that the high retention in white matter is largely attributable to slow PIB kinetics, while the opposite is true for putamen and other high flow areas. Paradoxically, the high accumulation in low flow areas potentially makes the methods more valuable to the diagnosis of AD because cortical flow rates consistently are lower in AD than in healthy control subjects. Here, we used a novel analysis of both flow-delivery and delayed washout by binding to obtain separate estimates of flow and binding.
Methods: We analyzed the difference, magnitude and distribution of the flow and binding components, and we compared the use of flow-normalized reference curves in the LL and RM methods to the flow independent HYPOTIME method for the imaging of the PIB-retention. The HYPOTIME method identified potential non-binding reference tissue directly from the data. Both healthy aged controls (HC) and patients with AD were tested with ^{11}CPIB and ^{15}O-water (for CBF validation).
Results: The initial wash-in peak value of the PIB signal relative to the reference region (R1 signal) correlated well with the gold standard R1 signal from ^{15}O-water. The R1 signal from PIB therefore served as a surrogate measure of the real R1. By normalizing PIB-derived R1 to injected dose and patient weight as well as calibration to a site specific factor, we obtained a surrogate measure of absolute CBF. Using the PIB derived R1, images were quantified in terms of binding potential and rate constants for the radiotracers before and after flow normalization using the LL, RM, and flow independent HYPOTIME methods. The flow difference between the AD and HC groups contributed significantly to the difference between the groups, with highly significant ($P = 0.0018$) reduction of cortical CBF in AD compared to HC subjects. This difference was independent of the use of the real or the surrogate CBF measure derived from the PIB scan.
Conclusions: This work shows that CBF is likely to confound any PIB-binding differences between the groups if not properly accounted for. The method also presents a simple estimate of relative (R1) and absolute (CBF) blood flow, directly from a single dynamic PIB session, by separation of specific binding from the flow-derived retention.